2005-07-07

Novel Neutron Detector for n-n Scattering Length Measurement

Eva Wilcox
Brigham Young University - Provo

NOVEL NEUTRON DETECTOR FOR n-n SCATTERING LENGTH MEASUREMENT

by

Eva Wilcox

A thesis submitted to the faculty of Brigham Young University in partial fulfillment of the requirements for the degree of

Master of Science

Department of Physics and Astronomy

Brigham Young University

August 2005

BRIGHAM YOUNG UNIVERSITY

GRADUATE COMMITTEE APPROVAL

of a thesis submitted by

Eva Wilcox

This thesis has been read by each member of the following graduate committee and by majority vote has been found to be satisfactory.

_____	_____
Date	Lawrence B. Rees, Chair
_____	_____
Date	J. Bart Czirr
_____	_____
Date	Manuel Berrondo
_____	_____
Date	Steven E. Jones

BRIGHAM YOUNG UNIVERSITY

As chair of the candidate's graduate committee, I have read the thesis of Eva Wilcox in its final form and have found that (1) its format, citations, and bibliographical style are consistent and acceptable and fulfill university and department style requirements; (2) its illustrative materials including figures, tables, and charts are in place; and (3) the final manuscript is satisfactory to the graduate committee and is ready for submission to the university library.

_____ _____

Date

Lawrence B. Rees
Chair, Graduate Committee

Accepted for the Department

_____

Ross L. Spencer
Graduate Coordinator

Accepted for the College

_____

G. Rex Bryce
Associate Dean, College of Physical and Mathematical Sciences

ABSTRACT

NOVEL DETECTOR FOR n-n SCATTERING LENGTH MEASUREMENT

Eva Wilcox

Department of Physics and Astronomy

Master of Science

The neutron-neutron (n-n) scattering length is a fundamental parameter in nuclear physics, but experiments give one of two different numbers and there is still no adequate explanation for this discrepancy. However, measurements are plagued with large uncertainties caused by neutron detector cross talk. Many experimentalists also rely upon computer code to calibrate their neutron detectors. We have developed a new neutron detector expressly for the purpose of improving the n-n scattering length measurement. It offers two important advantages: 1) minimal cross talk and 2) high counting efficiency. We calibrated the detector from 1 MeV to 6 MeV at 1 MeV increments. We have shown that the computer code, MCNP, does not always give the correct detector efficiency, and that reliance upon this code for calibration could be a large factor for error in previous experiments. Preliminary tests show no cross talk between two like detectors and suggest that these detectors are appropriate for a n-n scattering length measurement.

ACKNOWLEDGEMENTS

The author wishes to acknowledge Dr. Thomas Massey for use of the Edwards Accelerator Laboratory in providing monoenergetic neutrons for calibration and preliminary scattering measurements. She thanks Sara Pozzi at Oakridge National Laboratories for her help modeling with MCNP PolyMi code and the idea of using a single glass detector. Thanks also to the members of her committee and to Brigham Young University for their support and direction in this research project.

TABLE OF CONTENTS

LIST OF FIGURES

LIST OF TABLES

1. Introduction

An important tool for nuclear physics and materials analysis is the neutron detector. Like all instruments, it is subject to certain limitations. In particular, the neutron detector can be subject to data contamination in the form of cross talk between detectors. Cross talk happens as a single neutron creates a signal in one detector and then hits the other detector and causes a second signal, mocking the scattering of two interacting neutrons. This often occurs in nucleon-nucleon and neutron-neutron scattering experiments. The experimental value of the neutron-neutron scattering length is still not well determined, there being two distinct answers obtained through the course of many measurements. To work towards the solution of this problem, a new neutron detector has been designed, built, and tested. It is hoped that this detector will be used to repeat the neutron-neutron scattering length measurement with less error and thus resolve the problem.

1.1 Nucleon-Nucleon Scattering

Nucleon-nucleon (N-N) scattering provides physicists with a method to study the strong force, charge symmetry, and charge independence of nucleons. This is done through a comparison of singlet ($^1S_0$) scattering lengths, a_{NN}. These are related to the reaction cross section by $\sigma_{NN}=4\pi a_{NN}^2$, where a is the scattering length. Charge independence implies that neutron-proton (n-p), proton-proton (p-p), and neutron-neutron (n-n) scattering would all produce the same scattering lengths. Charge symmetry implies that n-n and p-p have the same scattering length (after making Coulomb corrections), the nuclear force being equal in both cases for the same state [1]. To date, accepted values of

the n-p and p-p scattering lengths are -23.71 fm [2] and -17.3 ± 0.2 fm [3] respectively. However, the studies of the n-n scattering length have not been conclusive. There are two values which frequently reappear: -18.6 fm and -16.5 fm, with large error margins of ± 0.4-6 fm. In order for charge symmetry to be valid, the value of a_{nn} is expected to be in the range from -16.6 to -16.9 fm [4]. The magnitude of the scattering length reflects the depth of the potential: for a just bound state the scattering length is infinite [5]. The negative values for the N-N scattering lengths are assumed to come from the attractive nature of the strong force and potential between nucleons. An attractive potential also indicates positive phase shifts in the scattering However, the number extracted from neutron spectrum measurements is a_{nn}^2, so only the magnitude is determined [5].

By comparing n-p and p-p scattering lengths, we see that charge independence is violated. The neutral and charged pion, and neutron and proton mass differences also show charge independence breaking [5]. It seems that we also have charge symmetry breaking [2]. To study charge symmetry breaking more closely, the n-n scattering length must be determined with more accuracy, and the discrepancy between the two values must be resolved. Quoting a textbook [1], "the study of p-p and n-n scattering also confirms the charge symmetry of nuclear forces." With the n-n scattering length unresolved, this is not the case!

Initially in singlet nucleon-nucleon scattering experiments, it was thought that differences in n-p, n-n, and p-p scattering lengths are due to $\pi^{\pm,0}$ mass differences [5,6], and were modeled with a one pion exchange potential (OPEP). However, the OPEP is only a good approximation for high angular momentum states, not singlet states [6], so the OPEP may be used for high-energy scattering experiments. Current theory for the

strong force includes heavier mesons with ρ-ω mixing [7] on and off shell, increasing the multiplicity of the equation. ("On the mass shell" means that scattering cross-sections are calculated using free particle mass, while "off shell" means that mass is reduced by binding energy.) Increasing multiplicity effectively introduces more terms with which to fit the data. Quantum chromodynamics (QCD) attributes the mass difference for the up and down quarks to charge symmetry breaking (CSB) [8]. In order to resolve these theories, we need a better measurement of the n-n scattering length, and to understand the cause of the discrepancy in the two measured values. It is important that we learn more about the neutron-neutron scattering length not only to understand more about the strong force alone, but to use that in astrophysics to better understand the behavior of neutron stars and other still denser forms of matter.

1.2 Neutron-Neutron Scattering Experiments

An indirect neutron-neutron scattering experiment was first proposed by Watson in 1952, to measure the photon spectrum from the reaction $\pi^- + d \rightarrow n + n + \gamma$ to find the scattering length. In his analysis he included a potential model which has been called the Watson-Migdal (WM) model [9]. Before this time, various potential models had been solved, such as the square well and the Woods-Saxon potential. These led to a variety of predicted scattering lengths, but since the potential was not well characterized, experimental n-n scattering measurements were needed to study the potential. Singlet scattering with low-energy experiments is not model-sensitive, but it is difficult to eliminate background in such low-energy measurements [5]. Direct n-n scattering with a free neutron target is not possible, but through colliding neutron beams or through

nuclear explosions, we could make a direct measurement of the n-n scattering length. At this point in time, no direct n-n scattering has been performed although many experiments have been proposed over the past 40 years [3], and a recent proposal has not yet been completed [3,10].

Many indirect measurements were done following Watson's proposal, primarily through two reactions, $\pi^-+d\rightarrow n+n+\gamma$ and $n+d\rightarrow n+n+p$. In order to perform an indirect measurement, the reaction must follow the form, $A+B\rightarrow C+2n$ [5]. This allows the two neutrons to interact with each other, where a reaction without a third body in the final state requires the neutrons to exit in opposite directions in the center of mass system, and preventing an interaction between the two neutrons. Neutrons interacting with each other in the final state influence the reaction cross section, and so these interactions are called final state interactions (FSI) [9].

In general, measurements from the $\pi^-+d\rightarrow n+n+\gamma$ reaction yield higher absolute values than those from $n+d\rightarrow n+n+p$. Let us look into the various indirect n-n scattering length measurements.

Table 1. Taken from Grötzschel et al. [11], neglecting those listed in Table 2. (1950-1970)

Reaction	a_{nn} (fm)	Ref. from Grötzschel [11]	Kinematics	Year
nd →nnp	-22 ± 2	[1-3]	incomplete	1964
	-23.6 ± 1.8	[4]	incomplete	1965
	-15 to -18	[5]	incomplete	1966
	-14 ± 3	[6]	incomplete	1967
	-16 ± 3	[6]	incomplete	1967
	-16.8 ± 1.0	[7]	incomplete	1968
	-15.9 ± 1.1	[7]	incomplete	1968
	-16 to -24	[9,10]	complete	1969
	-23.78	[11]	incomplete	1968
	-19 + 6,-12	[12]	complete	1969
	-23.2 ± 1.8	[13]	incomplete	1970

nt→nnd	-17	[15]	incomplete	1966
	-17 ± 2	[16]	incomplete	1968
	-18 ± 3	[17]	incomplete	1965
td→nn^{3}He	-16.1 ± 1.0	[18]	incomplete	1966
	-16.5 ± 1.0	[19]	incomplete	1969
	-18 ± 3 to -19 ± 2	[20,21]	incomplete	1970
dt→nn^{3}He	-14 to -22	[22]	incomplete	1967
tt→nn^{4}He	-16 ± 3	[23]	incomplete	1968
dd→nnpp	-15.5 ±1.1	[25]	incomplete	1970
π^-d →nnγ	-15.9 + 7.4, - ∞	[26]	incomplete	1954
	-12.6 to -24.7	[27]	incomplete	1964
	-13 ± 3	[30]	incomplete	1968

Table 2. Table from Bodek et al. [12] Table 2. (1965-1990)

Reaction	a_{nn} (fm)	Ref. from Bodek [12]	Kinematics	Year
π^-d →nnγ	-16.4 ± 1.3	[23]	complete	1965
	-18.42 ± 1.53	[24]	complete	1968
	-16.7 ± 1.3	[25]	complete	1975
	-18.5 ± 0.4	[2]	complete	1984
	-18.7 ± 0.6	[26]	complete	1987
$< a_{nn}(nn+\gamma)>$	-18.34 ± 0.31	sign. level = 0.36		
nd →nnp	-16.1 ± 0.9	[27]	complete	1972
	-17.1 ± 0.8	[28]	complete	1975
	-16.0 ± 1.2	[29]	complete	1974
	-16.8 ±1.3	[29]	complete	1974
	-16.3 ± 1.0	[30]	complete	1974
	-16.3 ± 1.6	[31]	complete	1975
	-16.9 ±0.6	[1]	complete	1979
$< a_{nn}(nn+p)>$	-16.63 ± 0.35	sign. level = 0.97		
dt →nn^{3}He	-16.2 ± 1.2	[32]	complete	1971
	-16.0 ± 1.0	[33]	complete	1973
$< a_{nn}(nn+^3He)>$	-16.08 ± 0.77	sign. level = 0.90		
tt → nn^{4}He	-15.0 ± 1.0	[34]	complete	1972
n^{9}Be →nn^{8}Be	-16.5 ± 1.0	Bodek et. al	complete	1990
$< a_{nn}$(nn+hadron)>	-16.40 ± 0.29	sign. level = 0.47		

Table 3. Most recent a_{nn} measurements (1998-2000)

Reaction	a_{nn} (fm)	Reference	Kinematics	Year
nd →nnp	-16.2 ± 0.4	[13]	complete	2000
nd →nnp	-18.7 ± 0.6	[14]	complete	1999
π^-d →nnγ	-18.5 ± 0.5	[7]	complete	1998

These tables comprise experiments using different reactions, potentials, final state interactions, and analyses. Kinematically "complete" or "incomplete" refer to knowing or not knowing all the final state kinematic parameters for each event, or detecting each of the outgoing particles [15]. In Table 1, which contains the oldest set of detecting experiments, we see a wide spread of values for a_{nn} even within given reactions. Notice in Table 2, which has only kinematically complete experiments, that there is a discrepancy between the $\pi^-+d\rightarrow n+n+\gamma$ and the $n+d\rightarrow n+n+p$ reactions. The Physics Report from 1989 [2] gives the recommended values from the $\pi^-+d\rightarrow n+n+\gamma$ reaction as $a_{nn} = -18.52 \pm 0.34$ fm, $r_{nn} = 2.80 \pm 0.15$ fm, and those from d(n,2n)p as $a_{nn} = -16.73 \pm 0.47$ fm and $r_{nn} = 2.85 \pm 0.60$ fm for the neutron pickup part of the reaction and $a_{nn} = -19.1 \pm 2$ fm for neutron knockon. [16].

Then, note in Table 3 the sudden discrepancy within the $n+d\rightarrow n+n+p$ reaction measurements. Previous to these recent measurements, the general belief was that the $n+d\rightarrow n+n+p$ reaction, having three nucleon forces, was less well understood and was not analyzed with a reasonable potential model. Let us look at validity of these experiments.

We can throw out all of the kinematically incomplete experiments. Currently accepted potentials for three nucleon forces like those involved in d(n,2n)p include the Argonne AV14, BonnB, Nijmegen-78 [17 ref. 29, 30, and 32], AV18+UIX, and Tucson-Melbourne (TM), [2,18,20]. The $\pi^-(d,2n)\gamma$ reaction scattering length extraction is less sensitive to model, so the Watson-Migdal [9] and McVoy [20] models may be used for $\pi^-+d\rightarrow n+n+\gamma$, and the Reid Soft Core (RSC) seems appropriate for this reaction as well [2]. Faddeev calculations with 3NF corrections [21] may be used with the Bonn-B potential for all three body processes. Many models often do not accurately predict binding

energies for the triton and alpha particles, making them unsuitable for use in modeling, and even the ones listed here still have limitations [2]. This rules out many of the listed experiments, and we are left with the following:

Table 4. Kinematically complete experiments analyzed with accepted models

Reaction	a_{nn} (fm)	Reference, Year	Model
nd →nnp	-16.2 ± 0.4	[13], 2000	Faddeev
nd →nnp	-18.7 ± 0.6	[14], 1999	Faddeev
π^-d →nnγ	-18.5 ± 0.5	[7], 1998	WM?
n^{9}Be →nn^{8}Be	-16.5 ± 1.0	[12], 1990	applied WM*
π^-d →nnγ	-18.7 ± 0.6	[22], 1987	RSC
π^-d →nnγ	-18.5 ± 0.4	[23], 1984	RSC
π^-d →nnγ	-16.7 ± 1.3	[24], 1975	McVoy
dt →nn^{3}He	-16.2 ± 1.2	[25], 1971	WM
π^-d →nnγ	-18.42± 1.16	[5], 1968	square
π^-d →nnγ	-16.4 ± 1.3	[26], 1965	square

*checked by measurement of a_{np} [27] to be an appropriate model for n+^{9}Be →n+n+^{8}Be

Note the clear distinction in results around -16.5 fm and -18.6 fm. We find both sets of numbers in both of the most commonly studied reactions, π^-+d→n+n+γ and n+d→n+n+p, and the other two reactions are both supporting the low number. However, theoretically, we have more confidence in the results from the π^-+d→n+n+γ reaction, as this reaction has no three-body forces in the final state interaction, which alter the potential in a way that has not yet been accurately determined. All the other reactions have a third strongly interacting particle, which need 3BF analyses. However, the n- γ interaction is negligible [20].

Von Witsch [21] gives an analysis and comparison of the two recent n+d→n+n+p experiments, concluding only that certainly only one answer is right. Notice also that the π^-+d→n+n+γ low values of a_{nn} came from older kinematically complete experiments. The square well model is considered acceptable here because both measurements are at

low energy or with the singlet state only, so the zero-range approximation is used. The neutron is insensitive to the details of the potential, and the width and depth of the square well can be adjusted, so almost any potential can be fit to the low energy data [5]. How do we determine which value is correct? And how will we resolve the discrepancy in scattering length values?

Recent reanalysis of kinematically incomplete n-d breakup experiments was made with 3NF Faddeev calculations [29,30]. Instead of resolving the issue of a_{nn}, the study shows a bigger spread in values, even beyond the error limits quoted by the original authors. In addition, this study notes a tendency for the values of a_{nn} to decrease with increasing incident neutron energy [28,29]. It claims to resolve the discrepancy with the $\pi^-+d\rightarrow n+n+\gamma$ reaction values if the cutoff parameter $\Lambda_\pi=5.9m_\pi$. However, our understanding of 3NF is at this time inadequate to draw any conclusions [7]. It has been asked if 3NF Faddeev equations are an appropriate tool in investigating breakup reactions [17].

1.3 Common Sources of Error and Possible Improvements

A general direct neutron-neutron scattering measurement would consist of either a neutron beam collision or a nuclear explosion, with neutron detectors adjacent or in line with each other. The general experiment for indirect scattering is comprised of a neutron or pion beam, a target to provide the reaction with two outgoing neutrons, neutron detectors adjacent or in line with each other, photon or gamma detectors depending on the reaction, and shielding. Of course, all of these bring systematic uncertainties to the experiment.

There are a few areas in neutron-neutron scattering which have long been causes of large error in measurements. While the theoretical uncertainties will have to wait for the development of better models or the completion of direct neutron-neutron scattering, we can do much to improve systematic uncertainties. These are neutron detector calibration, cross-talk between detectors, background scattering or room return, and neutron beam flux uncertainties.

It is possible that some neutron detector calibrations relied on computer modeling with Monte Carlo codes without referencing to any physical calibration, the worst case scenario. This is sound only if we can completely rely on the model to tell us how a physical detector responds to its environment. This thesis will address some inaccuracies of Monte Carlo Neutral Particle (MCNP) codes in section 5. To find an explanation and example of MCNP code, see Appendix 1. Some groups [11,12,13] did calibrate their detectors with one or two energies and then extrapolated using a model. This is not quite as bad, but still risky. A complete experimental calibration is necessary to be truly confident in the results, which two of the most recent measurements from Table 3 did [7,14]. A good calibration requires a few essential elements: a well calibrated source with a characterized spectrum, low background and room return, electronics system with a established dead/live time, and a accurate measure of the solid angle of the detector with respect to the neutron source. The efficiency is calculated by

$$\text{Efficiency} = \frac{\text{Detected Events Rate} - \text{Background Rate}}{\text{Incident Neutron Rate}} \qquad (1)$$

A very common problem with adjacent scintillation neutron detectors is cross-talk, where a single neutron is detected in both of the detectors. Again, most groups [7,12,13,24,25,30] have relied on modeling to take cross-talk into consideration, which may or may not be accurate. However, recently, a new detector has been developed which has no problems with cross-talk [31], as it is designed in a different manner than previous detectors; for details, see section 2.1. As cross-talk is one of the largest sources of error in these measurements, and this detector requires no modeling to account for it, it provides an excellent opportunity to make the measurements with more accuracy.

Room return comes from backscattering of neutron off of cement shielding, or any other thermalizing material. In a small room, room return can contribute as much as 50% of the detected signal to the detector. Often, computer modeling is used to determine the amount of room return affecting the experiment. One successful experimental means of accounting for room return is in running the experiment without the reaction, to acquire a background spectrum.

Neutron beam flux is often not known to within 5% accuracy, making another large source of error [32]. However, with a transfer standard, where the standard detector has been calibrated from the very well known d-d reaction, we can cross-check the flux and perhaps reduce the uncertainty, see section 7.1.

1.4 Proposal

We planned to use the reaction $n+{}^{9}Be \rightarrow n+n+{}^{8}Be$ to redo the experiment done by Bodek et al. with no cross talk, better background analysis, an active target, and a completely experimental neutron detector calibration [12]. The cross talk is eliminated

and background is less problematical because of the type of detector we use [31]. The active target is lanthanum beryllate. However, our active target did not respond as well as hoped, so we instead used deuterated benzene and the n+d→n+n+p reaction. Due to the time constraints of a master's degree, we prove the principle without completing the actual n-n scattering length measurement.

2 Detector Properties and Optimization

2.1 Introduction to the 1-L Coincidence Spectrometer

We based the detector on the previously developed spectrometer [31] which Dr. J. B. Czirr and Dr. G. L. Jensen designed at Brigham Young University (see Figure 1). This detector is composed of alternating layers of plastic and glass scintillators, in a cylindrical plexiglass container with a small amount of mineral oil for good optical coupling. The plastic container is 5 ¼" ID, 5 ½" OD. The glass plates were 1 mm thick, and the plastic layers are 1 ½" thick. These are both optically transparent, although the plastic scintillator takes on a slightly blue appearance. A 5-inch photomultiplier tube (PMT) is fixed to the open end, and then the whole apparatus is put inside a light-tight aluminum case. The plastic scintillator is BC408, the glass is a lithium-6 glass plate manufactured by Applied Scintillation Technology in the U.K. The PMT is attached to the container through use of vacuum pressure from the mineral oil inside, a tight connection being made by O-rings on each inside lip of an aluminum ring which fits the plastic container on one side and the PMT on the other. The O-rings are Viton which do not react with mineral oil [32].

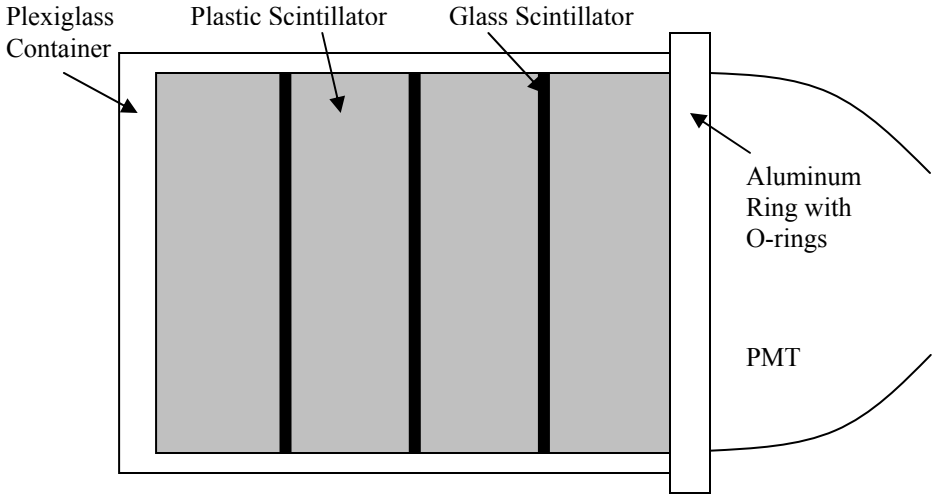

Figure 1. Detector components: side view

The plastic and glass scintillators provide recoil and capture pulses, respectively. Since this is a coincidence spectrometer, both pulses are required to indicate an event. An incoming neutron will have multiple collisions in the plastic scintillator with protons and carbon nuclei before being captured by lithium in the glass scintillator [31]. The plastic and glass each provide characteristic pulses. The pulse produced from the collisions within the plastic scintillator has a pulse area which corresponds to the total energy lost by the neutron. If a neutron loses nearly all its energy then it may be captured by lithium-6, which then decays and produces a characteristic pulse. The mean capture delay is 28 μs [31]. The pulse shapes are easily distinguishable, the recoil pulse being very fast and more or less symmetric, and the capture pulse being slow and with a long tail (see Figure 2). These capture pulses are roughly constant in size, as the lithium Q value, 4.8 MeV, is large compared to the kinetic energy of the captured neutron.

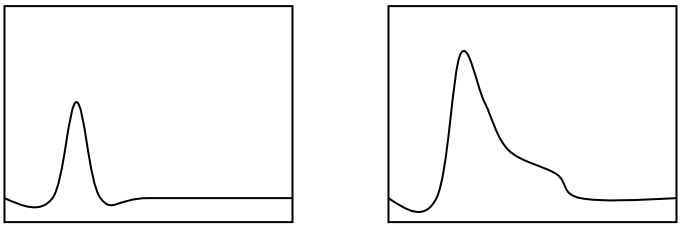

Recoil Pulse Capture Pulse

Figure 2. Recoil and capture pulses

The light pulses produced in the scintillator are then converted into electrical pulses in the PMT, which are analyzed in an electrical system. More discussion about electrical systems is found in Section 3.1. These double event detectors eliminate cross-talk because in order for a neutron to be counted, it must be preceded by a start pulse. If a neutron creates a start pulse in one detector and is captured in another, neither detector will recognize the event as valid.

2.2 Detector Optimization

Since we planned to copy the experimental setup of Bodek et al. [12], we wanted to optimize the detector for the neutron energies detected out of the $n+{}^{9}Be \rightarrow n+n+{}^{8}Be$ reaction. Bodek et al. [12] had energies from 2-6 MeV, so we set out to maximize the detector efficiency for incident neutron energy of 4 MeV by modeling with MCNP. Again, to see an example and explanation of MCNP code, see Appendix 1.

At first, we wished to limit scattering off of the aluminum container which houses the detector. The original casing is represented in Figure 3. It is approximately 8" in diameter and 1/4" thick in the middle, 8 ½" in diameter at the base and the top. The base

and top are 3/4" thick, with the base hollowed out to 3/16" for a 5" diameter circle, so that the incident neutrons scatter less and get inside to the detector. Inside the aluminum case are three aluminum screw rods which the plastic container sits inside. A metal ring with three holes fits over the top of the PMT, so that the screw rods can be used to enforce vacuum pressure inside the plastic container. The top of the aluminum can fits over all of this. Both the base and the top aluminum ends fasten onto the middle section with eight screws. At the top is a smaller ring, designed to fit around the base of the PMT, and screwed down with an O-ring in between the ring and the top piece of aluminum, so that the casing remains light-tight.

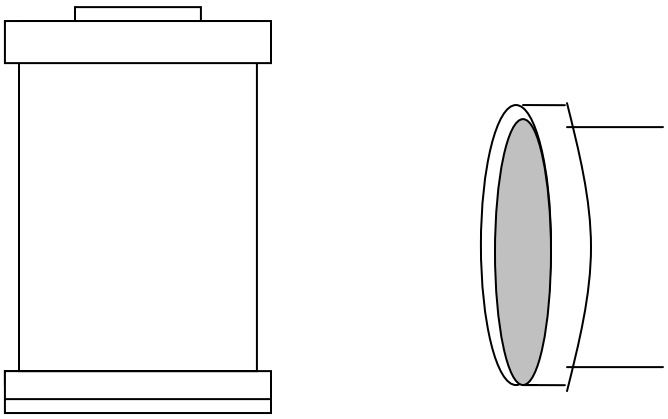

Figure 3. Original aluminum casing

In modeling the system, we noted that aluminum contributed about 2% to the overall detector efficiency (as reported by MCNP) and we wanted to minimize the contribution from aluminum. To do this, we redesigned the base and sides, so that less aluminum mass would be at the front of the detector. The new design has a 1/8" thick side, but a 1/16" base welded on to it, eliminating the need for screws and all the bulk of

aluminum that comes with them at the front of the detector. The new casing may be viewed in Figure. 4.

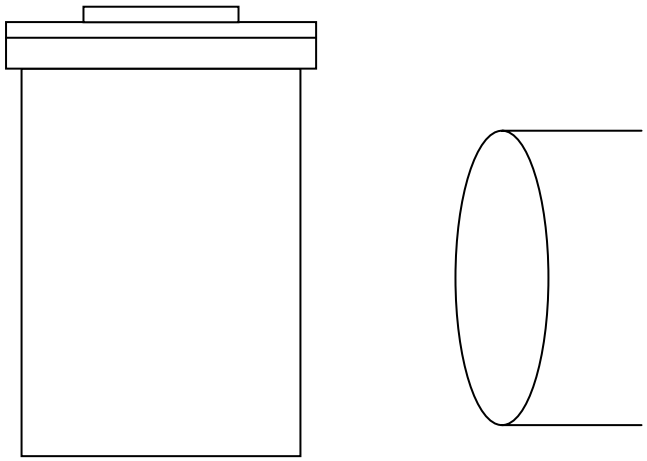

Figure 4. New design for aluminum casing

Figure 5. Detector, outside half-painted

Once the aluminum casing was redesigned, we next turned to thicknesses of the plastic scintillator. In order to make two identical detectors, we planned to use available glass scintillator sheets. We had to abandon the three circular pieces in the original detector. We instead used twelve square 10 cm x 10 cm pieces with rounded corners cut from glass from two other neutron detectors no longer in use. These were manufactured by the same company which was then called Levi-Hill LTD.

We found that the front piece of scintillator, if thinner, increased the detector efficiency. We cut the first piece of plastic scintillator to 3 cm thick. We also found that increasing the thickness of the last piece of scintillator would increase the efficiency, however, due to cost of thicker pieces of plastic scintillator and to ensure good light reception by the PMT, we left it at its original thickness. We also tested different numbers of glass plates, but three turned out to be the most cost effective for efficiency. For the first detector model, we continued to use the 1 mm thick circular glass plates from the original design.

Separate from MCNP modeling, the other changes we made to the system were to purchase two new Electron Tube, Ltd. (ETL) PMTs which have higher collection efficiency and speed than the Hamamatsu one we had been using.

We drilled and tapped a hole in the side of the plastic container. This is so that taking the detector apart does not require drilling a new hole and then repairing the hole each time we take apart the detector. We have to release the vacuum pressure from the mineral oil filling all empty spaces between the pieces of the detector inside. This hole is closed with a shortened stainless steel screw and another Viton O-ring so the mineral oil will not react and discolor. Eventually after a few preliminary calibrations, we painted the outside of the plastic container with reflective white paint to increase the efficiency.

The second detector that we made was not made identical to the first because the first piece of plastic scintillator was left 3.8 cm thick instead of cutting it down to 3 cm. In other respects they are identical. We did not correct the front thickness due to time constraints in shipping both detectors to Ohio. It will not have significantly different efficiencies from the calibrated efficiencies of the first detector.

3. Analysis Instruments and Methods

3.1 Electronics Systems

For our data acquisition, we used boards developed by David Buehler, an electrical engineer, under Dr. Czirr's direction. There are two types of boards: dosimeters and digitizers.

Dosimeters discriminate between types of pulses and record double events, i.e. the recoil and capture pulses, and reject all single pulses. They record fast and epithermal (slowed to room temperature) neutron captures, gamma pulses, and livetime. The neutron capture pulses it records are within a certain window after the start pulse. This timing is set for the borate capture window and not lithium, which occurs much more quickly after the recoil or start pulse than borate does. The dosimeter can be used in counting mode, highrate, or serial modes. Counting mode shows the recorded events separated into captures, gammas, and epithermal neutrons on the LED display, as does highrate, which runs with less deadtime. The LED display always shows the livetime for the run. The serial mode is used to send data into a computer with Comread, a data transfer program, to be analyzed on SCOPE. Serial and counting modes in the dosimeter are equivalent in data. Generally, the data analysis from the dosimeter comes from adding the recorded capture and epithermal neutrons, and dividing by livetime to get the rate.

The digitizer has the same modes and displays, but is used primarily in serial mode with SCOPE, and since it records all pulses there are no double pulse rejections due to timing as there is with the dosimeter. The digitizer, on the other hand, records all pulses, and doesn't order them into correlated start and stop pulses as the dosimeter.

Using the digitizer, we can count neutrons directly, instead of only ones which trigger a double pulse event. The double events are important when using the detector as a spectrometer because the start pulse area represents all of the incident neutron's energy. However, when not extracting the incident neutron energy but counting neutrons, the digitizer is sufficient and more inclusive when considering the pulse cutoff time, and thus is more accurate. For analysis with serial mode, we use a program called SCOPE to count the neutrons, and then use the livetime to find rates, as before.

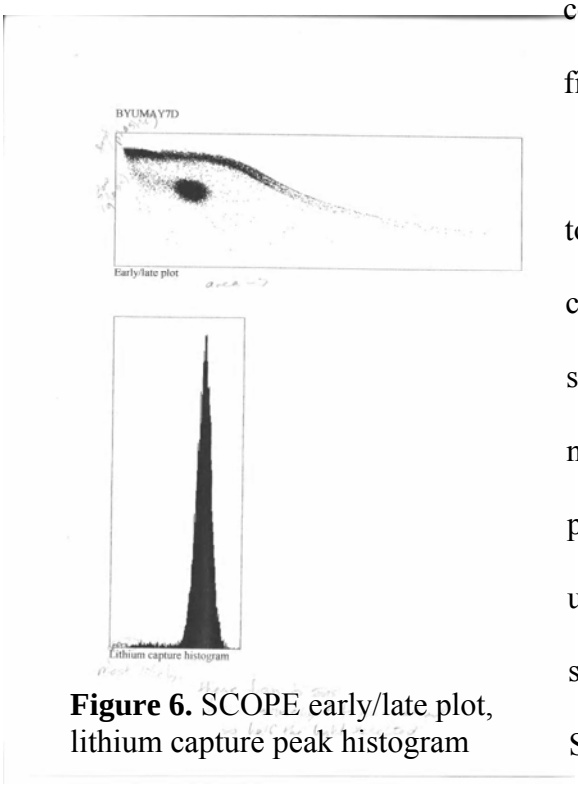

Figure 6. SCOPE early/late plot, lithium capture peak histogram

For our work with MCNP, it was important to use the digitizer so that all neutrons detected could be accounted for. For the actual n-n scattering length measurement, the dosimeter is necessary because with the coincidence, the recoil pulse (first detected pulse from neutron detector) is used as the stop pulse for TOF measurements, the start pulse coming from the active target (see Section 4.2). The neutron capture pulse (second detected pulse) ensures that cross-talk does not happen. If the neutron creates a collision pulse in one detector and is captured in another, the event is rejected, because there is a coincidence event in neither detector.

3.2 SCOPE, Comread, and Evecon

SCOPE is a computer program written to analyze data with both start and stop pulses. For a user's manual see Appendix 2. It reads the files created by the program Comread, from the digitizer or dosimeter in serial mode. SCOPE plots the pulses by the slopes of the pulse peaks (early/late) vs. total pulse area. Effectively, this separates neutron, proton, and gamma pulses, because of the differences in characteristic slopes and areas for the pulses. Proton pulses have steep slopes and small pulse areas and neutrons have smaller slopes and comparatively large pulse areas.

Because of the spatial separation on the plot, we can select regions of interest and perform more detailed analyses with them. In this way, we can count the total number of neutron events and look also at the histogram of the number of neutrons as a function of pulse area. Capture in lithium, for example, yields a sharp peak on the histogram.

The feature called configure dosimeter allows double events with a start followed by a stop to be written to an MeV file. An MeV file is one that can be read by Microsoft Excel. It contains information on pulse area, time between pulses, and event number for the start pulse. Double events are used whenever spectrum is important. Another computer program named Evecon allows the time specification.

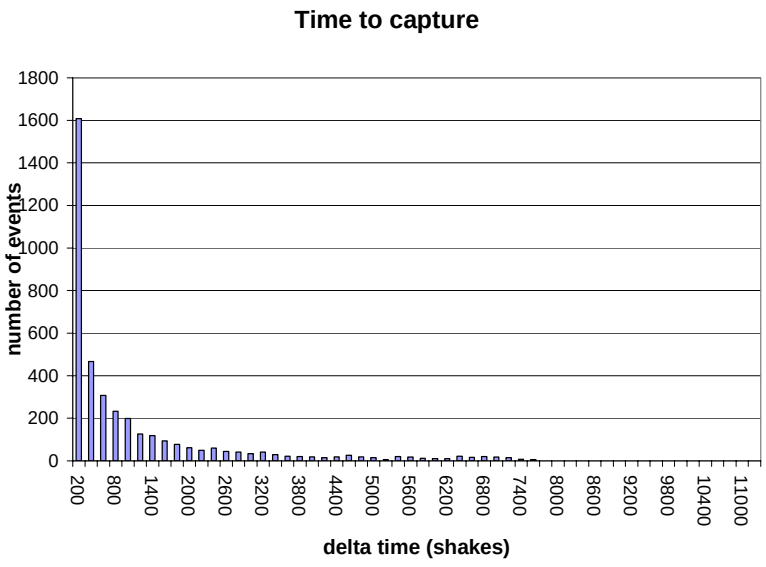

Figure 7. Number of events versus time

Comread by itself only correlates 13 μs worth of data. Evecon reads the Comread event files but allows a time specification on its display, so any range may be used. We can specify the time interval we desire for the recoil and capture pulses to be correlated as double. For lithium glass this time is 100 μs (see Figure 7). The mean capture delay for lithium glass is 28 μs.

3.3 Excel Analyses

Once we have an MeV file from SCOPE's "configure dosimeter", we can sort out the data in Microsoft Excel. We use Excel for any spectrum analysis. We have a program written in Excel by James Carroll, which bins the events into columns according to recoil pulse area. The recoil pulse area corresponds to the incident neutron energy. Thus a plot of these bins corresponds to the neutron spectrum. The size of these bins is variable, but we typically use a bin size of 100. The area units are defined by the Buehler boards. The binned recoil pulse areas comprise the detector response function.

These double events are also subject to time discrimination through the Excel file, so that we control the time window in which these events can reasonably occur. To find this time from start to stop pulse, we plot all of the double event times and see where the slope becomes flat in time. For lithium this time is approximately 100 μs, or 2500 shakes in the arbitrary electronic unit of the Buehler boards. 1 shake is 10^{-8} seconds. Figure 7 is created this way.

The accidental spectrum is also analyzed on Excel. Accidentals are the double events which occur not from combined recoil and capture event but from a random coincidence. To analyze their frequency we use double events which occur well beyond

the capture pulse time. For lithium glass, the longest capture decays at 100 μs, so we use 140-940 μs for accidental coincidence analysis. This is eight times bigger than the lithium glass time increment so that we may have good statistics. We can bin these events by recoil pulse area and obtain the spectrum. For the 1-L detector these events are not usually flat in time, but have a low energy peak around 1 MeV. After this spectrum is obtained, we may subtract 0.125 of it from the data spectrum.

3.4 Californium Sources

Brigham Young University owns two californium-252 fission sources. One was calibrated relative to a NIST standard on June 15, 2003. It had an activity of 490.0 μCi ± 3% on that day, which is equivalent to 2.103 x 10^6 neutrons/second, as the accepted conversion between the two units is 4.292 x 10^3 neutrons/sec/ μCi of ^{252}Cf. The other is probably 30 years old, and it is now a weak neutron source. The half life for californium-252 is 2.646 years. The spectrum is well known [33] (see Figure 8).

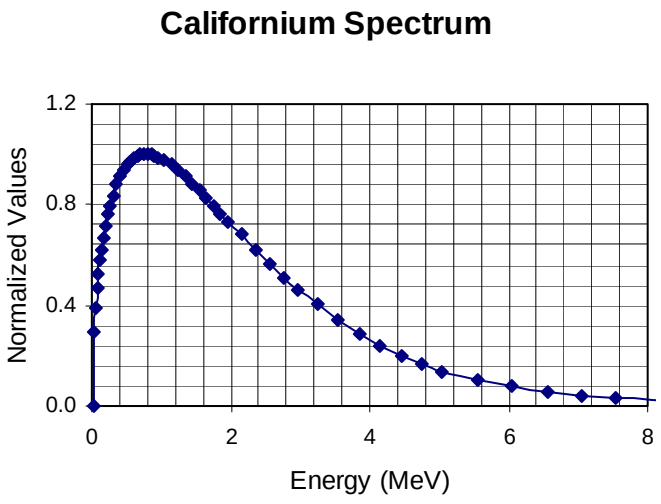

Figure 8. MCNP californium spectrum [33]

The weak californium-252 source is inside of a steel tube 0.5 mm in diameter, and 3 cm long. In order to test which part of the tube housed the fissioning material, we made a thin window with lead bricks

and used a sodium iodide counter. We moved the tube, allowing us to find the position for which we detected the maximum number of neutrons. The source turned out to be right in the middle of the tube, and not at the ends. The new calibrated source is a small capsule, perhaps a steel covered capsule but thin enough to not affect the emissions.

3.5 PMT Voltage and Gain Optimization

Initially we employed the dosimeter, and the histogram from SCOPE to determine the lithium peak for different voltages on the PMT. 1600 V produced a histogram with the low energy side of the peak cut off because of the threshold value in the Buehler board. 1700 V saturates the detector if the weak source was not beyond two feet away from the detector, so we chose 1650 V, using threshold values for baseline of 12 and early/late cut of 20. However, when the weak source was put within 30 cm of the detector, as is necessary for mounting the system in the Marriott Center, the electronics were again swamped. By changing the threshold values, we found that a baseline of 12 and early/late cut of 25 worked well at 1600 V. These values were used for the Hamamatsu tubes. Later on we switched to ETL tubes and had to repeat the process for each tube.

With the same process repeated for the first ETL tube, we found 1300 V was necessary, and for the second tube it required only 1100 V to position the lithium peak in the same place on the early/late plot in SCOPE.

3.6 PHA

The pulse height analyzer was used as an independent check on the Buehler boards. It is manufactured by Toshiba , Model T6600C. Running into the PHA requires a preamplifier to amplify the signal from the PMT. It takes each pulse and distributes it by pulse height, running in a summing mode. In time the picture for a lithium capture peak develops into a decaying exponential with a small peak representing the lithium captures, which are roughly constant in height and shape. The PHA has a deadtime much smaller than the Buehler boards for the same source and source distance.

4. Calibration with Californium-252

4.1 Addressing Suitable Room Return and Electronics System

The next step was to calibrate the detector with californium-252. In our facility, the nuclear physics group uses an underground laboratory, with cement shielding two feet thick and eight feet high surrounding the area in which we use radioactive materials. Generally for calibrations, the detectors are placed a few feet off the floor, with the californium fission source a foot away from the detector.

The 1-L detector was the second in line to be calibrated that summer; the first was a lithium gadolinium borate (LGB) detector [34], a detector 2 inches in diameter and 2 inches tall, attached directly to a 2-inch PMT, encased in a thin aluminum container for light-shielding. We used a dosimeter for the data acquisition, which collects double events of recoil pulses followed by neutron capture pulse. To calibrate, we subtract the background neutron capture rate from the detected neutron capture rate with a californium source, and divide by the incident neutron rate on the detector as found from the radioactive decays and the solid angle. This measurement was found to be in good agreement with the MCNP calculations, approximately 15%.

However, the same measurement was performed at NIST with an identical detector, and they arrived at a completely different, much lower efficiency. In comparing the two calibrations, NIST was attributing half of their data to room return. We decided to move the experiment away from all concrete surfaces, and built a ‘massless’ tower of cardboard boxes to support the system in the air. The calibration was run again, and we arrived at yet another efficiency, but even though the detector was now 6-7 feet from any cement, the back-scattering of neutrons from the cement still contributed about 20% of

the detected neutrons. All estimates of background effects come from MCNP by approximating a spherical shell of cement with radius of the closest distance, and comparing the efficiency with the efficiency of a run with no cement.

The background problem would be even more dramatic in the large detector, so we needed to find a facility with enough open space to allow a background rate of 1% or less, so we could lower the systematic correction. It is Dr. Czirr's preference to never have more systematic error than statistical error. By increasing the room size, we increase the distance from the cement to the detector, which decreases the room return from each point of the cement by $1/r^2$ for a spherical approximation. Brigham Young University has an indoor auditorium, the Marriott Center, which has plenty of open space. We were able to make arrangements to use this facility for our measurements.

The other problem which concerned us is the disagreement with MCNP. We thought of these possible problems: that our understanding of electronics livetime was in error, our modeling of the aluminum container over the LGB detector could be inaccurate, the estimate of room return was faulty, that we were missing some real events that were not being picked up by the electronics (dosimeter), or perhaps multiple neutrons were counted as one or zero neutrons. We tried modeling with and without cement with 100 million neutrons without being able to resolve the issue.

The calibration of the small borate detector was performed with the new, calibrated, californium source. Were we to use the new source with the 1-L spectrometer at a distance allowed by the mounting system, the rate of capture in the detector would flood the electronics, raising the deadtime to over 90 %. This would make high error in measurement more likely. This meant that we needed to use either the weak source or

increase the distance between source and detector which would cause problems with mounting the system in the Marriott Center and increase the background level. We calibrated the weak source against the new source, so that we would know the activity of the weak source to use in calibrations.

To do this, Dr. Czirr used two different types of analyzing systems for neutrons and gammas: pulse height analyzer and the Buehler boards. Both yielded the same ratio of activities with the neutron measurements, to within 1% accuracy, which is even a smaller error than that of the initial calibration of the new source. The small borate detector was used for this purpose so that the electronics would operate in the linear regime. The ratio of the activities of the weak to the calibrated ^{252}Cf source is 0.019358., or about one-fiftieth. By this we could also check that our source was not flooding the electronics into nonlinear regions with more efficient detectors such as the 1-L detector. By checking the rates for both sources at a certain distance, when the ratio of strong to weak is less than fifty, the strong source causes nonlinearity in the digitizer, and we can adjust accordingly.

To check the spectrum of the old source, which may have shifted because of the decay products, we asked a specialist at NIST to resolve this question. He told us that the decay products are all short lived when compared to californium, so it doesn't shift the neutron spectrum at all, and the gamma spectrum should not shift significantly.

4.2 Marriott Center Calibrations

Brigham Young University has two buildings that have adequate space to be useful for calibrating our detectors with very small room return: one is the Marriott

Center, an indoor auditorium seating 22,000 people, the other is an indoor intramural sports field. We also had the option of using an outside facility, which we first considered but dismissed due to weather considerations. We decided to work through the Marriott Center (see Figure 6). We used a catwalk to hang the detector approximately 30-40 feet from the floor, which was the closest surface. It is 100 feet from the catwalk to the floor, so we used a 200 foot rope and 40 foot electrical cables to lift the system to the appropriate height. We first used a lightweight aluminum garbage can lid for mounting the detector and source.

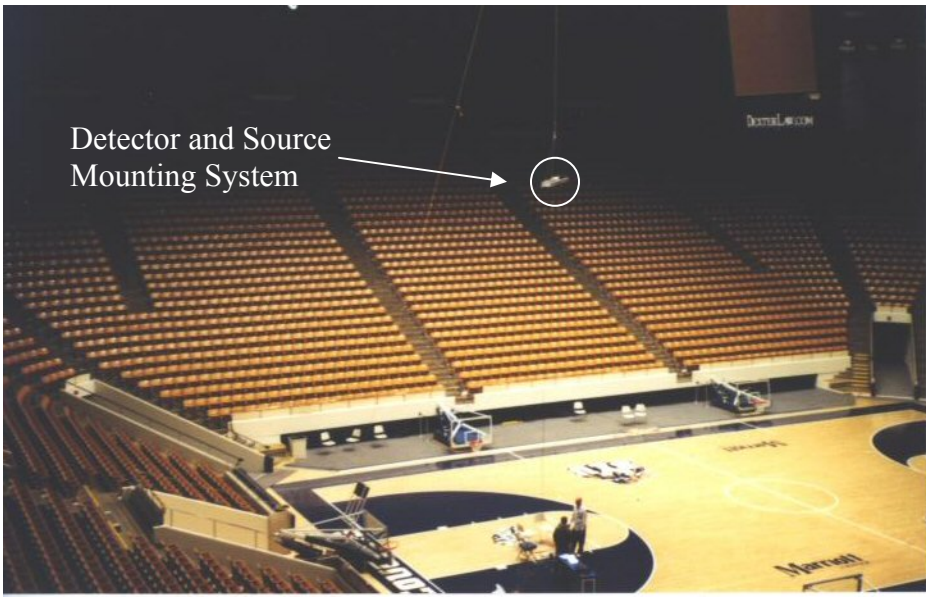

Figure 9. Marriott Center calibrations

This time, we were able to calibrate the small borate detector very accurately. We obtained an efficiency larger than the one calculated at NIST, but background was measured separately with the source not mounted, and room-return was calculated to contribute only about 1% to the background measurement. We now had a facility we could use for calibrating the 1-L spectrometer. Our only concern was for the

disagreement of MCNP to the LGB measured efficiency, which was now twice as large as the measurement.

4.3 Initial Calibration of the 1-L Spectrometer

Calibrating the 1-L spectrometer proved more difficult than we had expected, due to the electronics system we use. We had not considered the allowed time between recoil and capture pulses to be a problem with the dosimeter, so our first run in the Marriott Center gave us a calculated efficiency a bewildering quarter of the value from MCNP. We started to investigate the matter with alternative electronics systems.

Through a comparison of data from both the digitizer and dosimeter, we were able to establish that indeed we were losing pulses due to timing cutoff with the dosimeter. The ratio between the two rates (after background subtraction) for the same source and source distance was 1.59, digitizer over dosimeter. The dosimeter was designed with timing cutoffs for LGB, not lithium glass. From then on, we used the digitizer in serial mode with SCOPE to get data for the 1-L detector. Now, since we had made the lithium capture peak studies to determine optimal voltage for the PMT with the dosimeter, we needed to check and see what was suitable for the digitizer. Repeating the process used with the dosimeter, we found that a voltage of 1800 V on the Hamamatsu PMT was appropriate with the weak source at 40 cm, using in the SCOPE analysis 12 and 25 for the baseline and early/late cut parameters, respectively.

Calibrating at the Marriott Center once again, we obtained an efficiency lower than MCNP. This was also true for the small LGB detectors, both 2” and 3”. Each detector had an MCNP efficiency approximately 140% of the measured. To probe the

matter further, we studied simplified systems. In modeling, we included the mounting systems and cement walls. For the 1-L detector we used a different mounting system. Using an electrical wire carrier six feet long, we attached the detector with clamps and the source with a thin aluminum stand, then clamped cables to each corner and to the rope to hoist it in the air (see Figure 10).

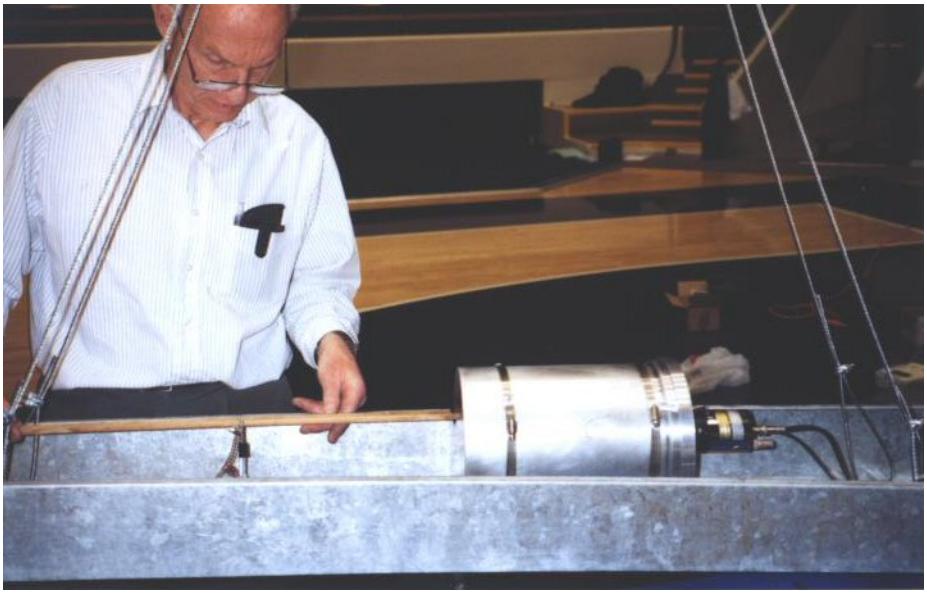

Figure 10. Mounting system with 1-L detector and Dr. J. B. Czirr

We put a single piece of glass scintillator on a PMT, and using the new californium source, looked at the lithium capture peaks on both the digitizer and the Pulse Height Analyzer (PHA). Doing this, we studied the lithium peak shapes on each system, and after a rough background subtraction, the ratio between the PHA and digitizer counts is 1.006. This establishes the error in MCNP, since the digitizer and the PHA both give the same answer.

We contacted an MCNP specialist, Sara Pozzi at Oakridge National Labratory, to discuss our results with her. She informed us that the LGB detectors are too complex to

use MCNP modeling for calibration. For the 1-L detector, she was sent all the data, and had the system geometry explained to her so that she could write and test a program independently. She also suggested we test a simpler system with only one piece of glass, and find the lithium content of that piece specifically.

4.4 Single Glass 1-L Spectrometer Calibration

To test MCNP's ability to predict efficiencies of simple systems, we prepared a new detector with two 5 mm thick pieces of plastic scintillator, a square plate of 2 mm thick glass scintillator, housed in the plastic body of the 1-L spectrometer. The glass was sandwiched between the plastic pieces, and spaced in the middle of the detector body by using narrower acrylic tubing, 4 ½" outer diameter, 4 1/4" inner diameter. The bottom piece was 7.2 cm tall, the top piece 7.5 cm tall. The empty spaces were filled with mineral oil. The single piece of glass was ground up and tested to determine the precise content. Since all the other square pieces of glass came from the same manufacturer and would only differ by small amounts, we then assume a linear relationship between light output and lithium content for the remaining square pieces of glass.

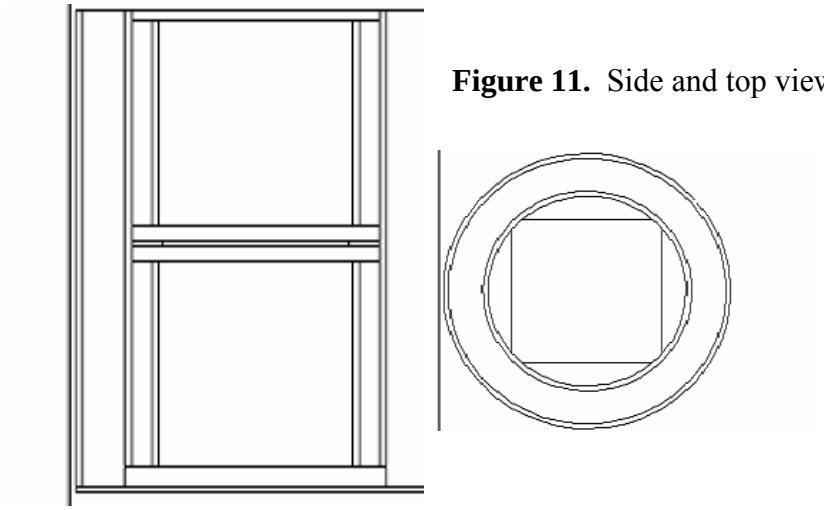

Figure 11. Side and top views of single glass detector

4.4.1 MCNP Calculation

We needed to know two specific things for an accurate MCNP calculation. The first is the precise lithium content of the glass, and the second is the mineral oil density.

The glass was ground up at Photogenics, and sent to Wiltec in Provo, Utah for dissolution. Neil Giles dissolved the glass with approximately 50 % HCl, and 50 % HF to completely dissolve the sample. He then diluted the solution to less than 0.5 % HF by weight, 0.3 % HCl, with a dilution factor of 3246:1. The lithium content analysis was done by BYU Chemistry Department, with an inductively coupled plasma atomic emission spectroscopy (ICP) analysis performed by Robin Parker. The instrument itself is the Spectrometer Model 2000 DV, which was run in the ICP Continuous mode. This analysis required a set of standard solutions to be made with the appropriate amount of HCl and HF, which were prepared with help of Dr. David Tingey from the BYU Geology department. We used three lithium standards with 9.9 ppm, 29.7 ppm and 49.5 ppm, and a blank with 0 ppm. The analysis showed a lithium content of 17.2 ppm, which converting back with the dilution factor is determined to be 5.597 % by weight in glass, with an error less than 1%. This result is consistent with a separate analysis performed by Enviropro Laboratories in West Valley City, Utah. Enviropro dissolved the glass in aqua regia, and found the lithium content to be 5.595 % by weight, with an uncertainty of ± 5 %.

Because the detector body is filled with hydrogen rich mineral oil, we also needed the precise mineral oil density or hydrogen carbon ratio. Tom McKnight determined mineral oil to have a hydrogen carbon ratio of 44:21. This information combined with the precise lithium content ready us for a precise MCNP calculation. The next step is to

precisely model the geometry of the calibration itself. The difference in modeling for the two sources lies in the precise source distance from the detector. Results are reported in Table 6.

4.4.2 Calibration of the Single Glass Spectrometer

We returned to the Marriott Center for this calibration. We used both sources so that we could check our accuracy. Background was taken when the sources were across the building, with many feet of cement in between them and the detection system. The source distances for strong and weak were 61.11 cm and 62.16 cm respectively. Height from floor was 13.9 m. The analysis was performed with SCOPE, choosing a region of interest around the lithium capture peak to count the neutrons. We did not use any Excel analysis. At first, we had 5 % disagreement between the strong and weak source answers. Alan Carlson at NIST suggested that perhaps we had some gamma pulses leaking into the neutron region. Californium emits roughly three gammas to every one neutron. To study this possibility, we used a radium button. Radium 226 emits gamma rays and no neutrons. Because there are no neutrons, we used the radium source in the underground lab with no fear of scattering. We took a background run and source run. The gamma leakage contributes approximately 6 % to the lithium capture region. This was determined by normalizing a certain region of gammas for both the radium and the californium runs. The ratio of counts in a definite lithium capture region from the radium to the californium represents the gamma leakage. Now, to account for background, in addition to subtracting the normal background rate, we had to subtract the counts in the gamma region times the ratio of the differences between the gamma rate and its background rate for the neutron and gamma regions. In equation form, this is

$$Eff=(1/R_{Si})(R_N-B_N-(R_G-B_G)(R_{\gamma N}-B_{\gamma N})/(R_{\gamma G}-B_{\gamma G})) \quad (2)$$

The R_G-B_G term acts as normalizer, and $(R_{\gamma N}-B_{\gamma N})/(R_{\gamma G}-B_{\gamma G})$ gives the gamma leakage (approximately 6 %, varying with the type of analysis). Eff stands for absolute efficiency, R_{Si} is the incident neutron rate on the detector, R_N is the signal rate in the neutron region, B_N is the background rate in the neutron region, R_G is the signal rate in the gamma region, B_G is the background rate in the gamma region for the californium runs, $R_{\gamma N}$ is the signal rate for radium in the neutron region, $B_{\gamma N}$ is the background rate for the radium run, $R_{\gamma G}$ is the signal rate for radium in the gamma region, and $B_{\gamma G}$ is the background rate for the radium in the gamma region. In other words, R stands for signal rate, B for background rate, G for gamma region, N for neutron region, and γ stands for radium runs.

We used this equation in four separate analyses: two with the strong source and two with the weak source. Each was analyzed with two separate sets of regions of interest in SCOPE, the left side of the region being the variable. For both sets of regions, the neutron region of interest had top =158, right =190, and bottom =100. For the gamma region we used top =200, right =190, and bottom =165. The left side for both gamma and neutron regions was either 60 or 96. This changed how the lithium capture peak was defined.

Table 5 lists the data, and Table 6 has the results. Rates are found by dividing counts by livetime. The neutrons incident on the detector, R_{Si}, was 1.59 E+6 n/s for the strong source, and 3.08 E+4 n/s for the weak source. The error for all ratios of measurement to MCNP is estimated to be less than 2 %.

Run	Livetime (sec)	N. Counts 60-190	N. Counts 96-190	G. Counts 60-190	G. Counts 96-190
Strong Cf	226	60384	57585	68232	40318
Weak Cf	8592.9	55458	50333	145019	80459
Bkgd Cf	6786	7736	5189	57357	35310
Radium	7575	26799	13258	333341	203583
Bkgd Ra	69560	36992	20104	305193	187168

Table 5. Single glass efficiency calculation data

Analysis	Measured	MCNP	Ratio Meas/MCNP
Strong 60	1.531 E-4	1.626 E-4	0.942
Strong 96	1.530 E-4	1.626 E-4	0.941
Weak 60	1.517 E-4	1.626 E-4	0.933
Weak 96	1.571 E-4	1.626 E-4	0.966

Table 6. Single glass absolute efficiencies by analysis

The measured efficiencies are very similar to each other. The average of the two weak source analyses is within 1 % of the strong sources. The weak 96 analysis being 3 % higher than strong source analyses gives a limit on deadtime errors from the electronics, since the strong source and weak source have a ratio of 50 in neutron emission rates. This study identifies the limitations of MCNP in reporting absolute efficiencies, the average ratio being 0.945 for the broad spectrum californium source. Thus the calibration of the 1-L detector with monoenergetic neutrons became essential for the n-n scattering experiment, as MCNP is more likely to be inaccurate with only one energy of neutron, and at much higher energies than the peak of the californium fission spectrum. On the other hand, a 5.5% difference between californium calculations and measurement gives us more confidence that our electronics collect all of the neutron capture pulses.

5 Ohio University Accelerator Monoenergetic Calibration

5.1 System Description

The detector was calibrated in 1 MeV intervals from 1.0 MeV to 6.0 MeV, for a total of six energies. The purpose of calibrating the detector in this region is to repeat the n-n scattering length measurement done by Bodek et al. [12] with the $n+^{9}Be \rightarrow n+n+^{8}Be$ reaction. The calibration was performed at the Edwards Accelerator Laboratory at the Ohio University in Athens, OH, with the help of Dr. Thomas Massey. Energies 1-3 MeV were obtained using the reaction $p+^{15}N \rightarrow n+^{15}O$, with energies 4-6 MeV from the $d+d \rightarrow n+^{3}He$ reaction. 1 MeV data were taken with an amplifier and the PMT at 1300 V to ensure that the recoil peak was above threshold. 2-6 MeV data were taken with no amplifier and 1200 V on the PMT, so that saturation of the pulses in the recoil peak would be less.

The accelerator at Ohio University is a tandem accelerator. We used a shielded beam in a long tunnel. This tunnel is lined with concrete, but the beam would not hit the concrete until the end of the tunnel, more than 25 m long and far enough away that room return is negligible. Our detector sat 5.9096 meters from the gas cell source, with the monitoring detectors back another meter at 6.932 meters from the gas cell. The 1-L detector took approximately 1/3 of the field of view, with two monitoring detectors in the other 2/3. These monitors are composed of liquid scintillator for the neutron detection, inside an approximately 20 cm diameter PVC pipe. These are the detectors used for the time of flight analysis of beam spectra. Before hitting the detectors, the beam travels through a collimator and borated plastic shielding to prevent background radiation and beam non-uniformity.

We used low-loss BNC cables to transfer data to the digitizer, so that the electronics would not alter the shape or amplitude of the pulses. The digitizer was run in serial mode into the computer using Comread.

A pulsed beam was used to determine the spectrum with time of flight analysis. The calibration data were obtained in continuous beam mode, due to the nature of the spectrometer. Each of the TOF spectra shows that the intensity at the peak energy is two orders of magnitude higher than the off-peak intensity (See Figure 12 for all spectra). Note that 1 MeV is not well detected by the liquid scintillator, and thus is at the limit of measurement and has the highest errors associated with time of flight. This means it is difficult to achieve good statistics at that energy because of the difficulty in measurement.

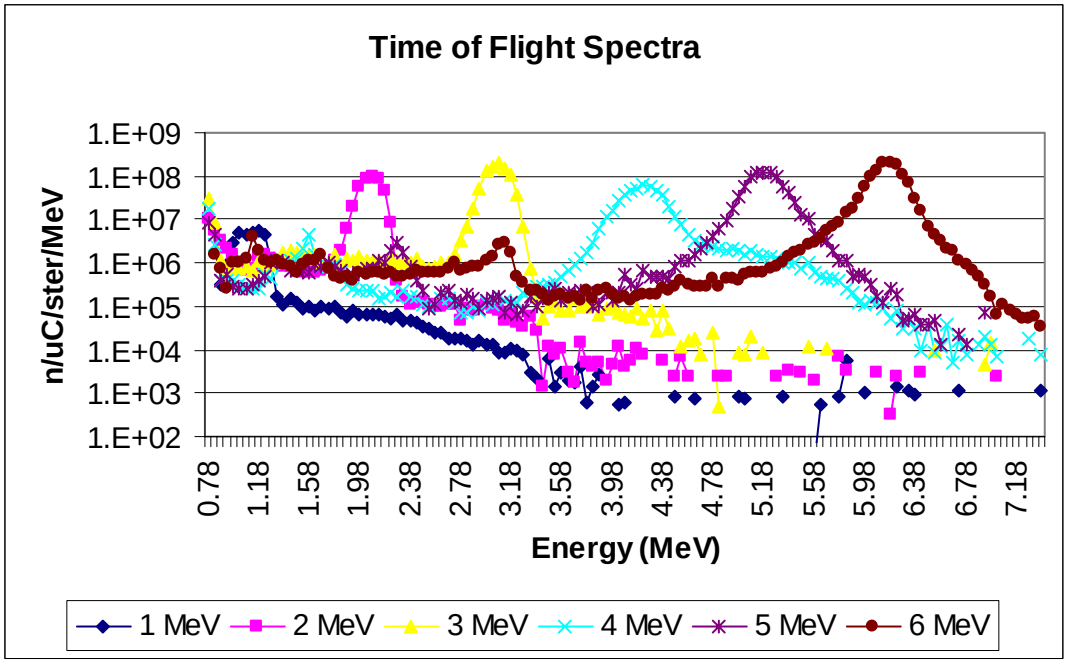

Figure 12. Ohio measured TOF spectra for 1-6 MeV

5.2 Data Analysis Methods

We used Evecon with the Comread event files to allow correlation of recoil and capture pulses in time. With SCOPE, we analyzed all the data with a baseline of 12, and early/late cut of 25. For 2-6 MeV, we set the SCOPE neutron capture region with left =25, top =125, right =153, and bottom = 65. The two proton recoil regions were set (numbers listed in same order) as 0, 208, 241, 125 for the first region and 153, 125, 616,

Figure 13. Data after background and accidental subtraction

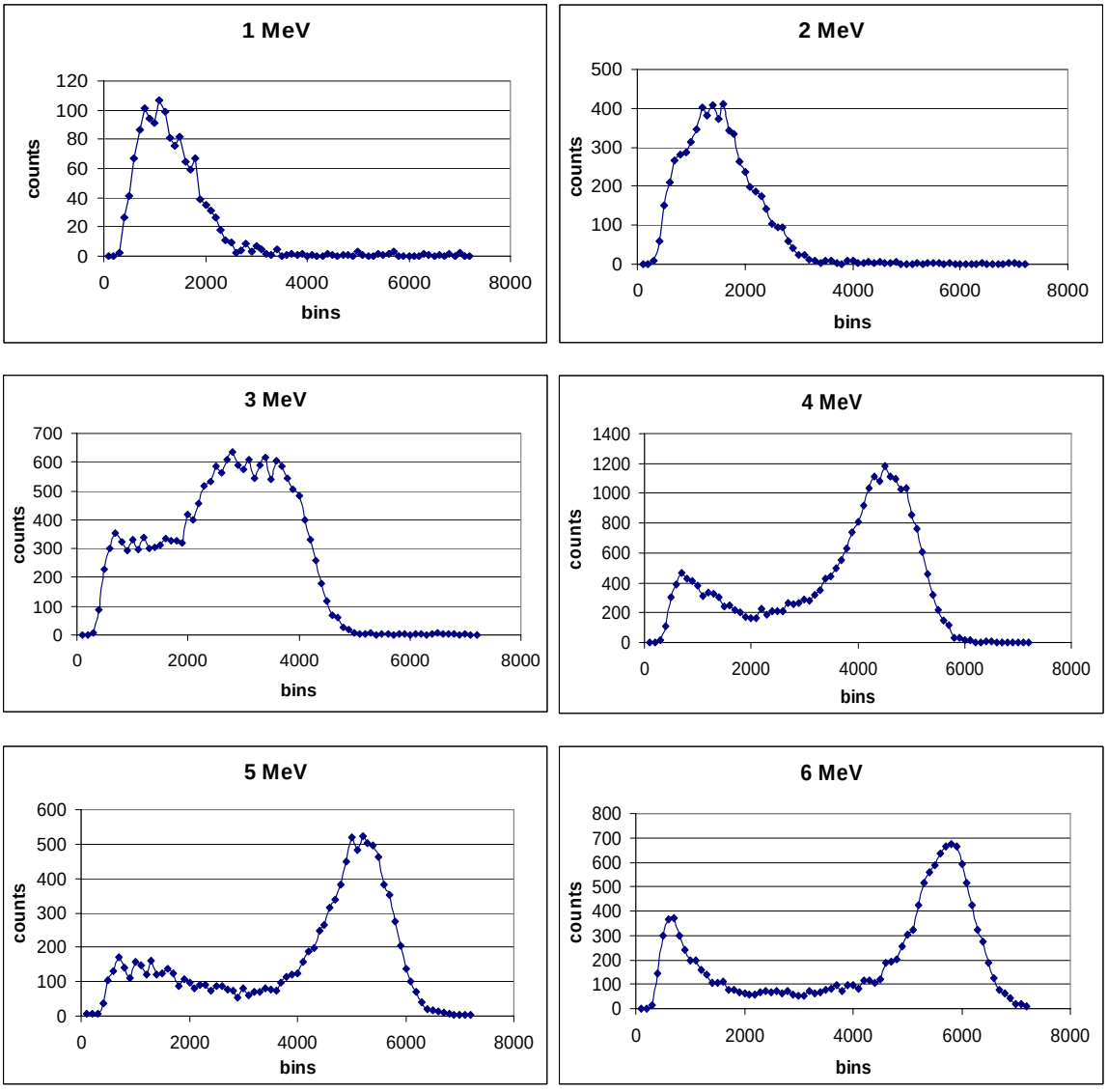

40 for the second. We used two regions to make sure that we picked up all of the events corresponding to the calibration. In general, we did not gain many events from the region to the right of the recoil peak. For 1 MeV, the regions of interest in the order of neutron capture and the two recoils are: 152, 88,284, 56; 0, 208, 360, 88; and 284, 88, 616, 46. We compiled all of the double events for each calibration in the Excel spreadsheet. We chose 100 area units for binning increments because it gave enough detail to show change in slope, while it is large enough not to show every random fluctuation.

The detector acts as a spectrometer with the main data peak moving to the right for higher energies. The response functions each exhibit a low energy peak. These response functions were created from an Excel analysis. Coincident events were allowed for 100 μs (see Figure 7). The accidentals were analyzed from 140-940 μs, and 0.125 of this spectrum was subtracted from the data. The background run at Ohio had a very small data acquisition rate, making the background negligible.

As evidenced by the response functions, the 1-L detector may be used as a spectrometer. However, we cannot yet explain the low energy peaks. 4-6 MeV data show us that the low energy peaks seem independent of energy, and that they are almost certainly present in 1-3 MeV data. Sara Pozzi at Oakridge National Laboratory informs us that computer modeling exhibits a low energy peak as well [35].

Monte Carlo N-Particle Transport Code System to Simulate Time-Analysis Quantities MCNP (MCNP PoliMi) modeling [36] of the spectra by Sara Pozzi at ORNL shows that these peaks are real and inherent to the system. This code is able to simulate recoil spectra of detected neutrons. She removed the aluminum casing in the model, then the carbon, and still the low energy peak remained. Although we do not know exactly

where the peak comes from, we do know some things about where it does not come from. It does not come from certain energies of neutrons, since it appears in all cases. It is not a function of incident number of neutrons, since the ratio of neutrons in the big peak to low energy peak is the same order of magnitude and there is no trend. It is not caused by the saturation in the electronics, because there are no electronics in the modeling, yet the low energy peak is still present. Even though the large peaks for 5 and 6 MeV are not symmetric with a steeper slope on the right side, the near symmetry of the 4 MeV peak gives us no reason to believe that the low energy peaks have any saturation effects at all. Because of Sarah Pozzi's modeling, we know the low energy peaks are not due to scattering from aluminum, nor due in any way to carbon elastic or inelastic scattering.

5.3 Efficiency Calculations

For 4-6 MeV, efficiency could be defined in one of two different ways. We could consider all counts in the spectrum as "good counts" or we could consider only the counts in the high pulse area or high energy peak as "good counts." The first method is a better measure of the actual efficiency for neutron detection; however, it is sensitive to details of how the low energy peak is cut off both experimentally and computationally on the low energy side. A more practical working definition of efficiency is to consider only the counts in the high energy peak. When considering how to calculate efficiency with this second method for 1-3 MeV, we must subtract the low pulse area peak. The shape is roughly the same for 4-6 MeV, so we assume that it also is the same for 1-3 MeV. The maximum for the peak occurs at the same energy (or in the same bin) for 4-6 MeV, so we

thought that this would also be suitable for an approximation for 1-3 MeV too. We need the total number of neutrons which were incident upon the detector to find the efficiency.

5.3.1 Determining the Number of Incident Neutrons

The Ohio time of flight (TOF) data gives us the neutron energy spectrum for each energy at which we calibrated the detector. These are given in counts per microcoloumb per steradian per MeV. We multiply this number by 0.05 MeV, the solid angle, and the total charge to calculate the number of incident neutrons. To a first approximation, we may take the sum of all the data in the peak of the TOF spectra (Figure 12), which represents about 95 % of the incident neutrons. For completeness, I used the sum of all the data from the TOF spectra at each energy. We will also assume that the all of neutrons in the peaks of Figure 13 are real data due to the subtraction of accidentals. To calculate the solid angle, we take the ratio of the cross sectional area of the detector to the surface area of the sphere created at the plane of the detector with respect to the source. The distance from the source to the detector is 590.8 cm, and the radius of the detector is 7 cm. Data from each continuous run provides information concerning the total charge accumulated during the run, in microcoulombs. Below is a table with all this information. Error is negligible.

Energy	n/(ster*MeV*μC)	μC	Steradians	Total Incident Neutrons
1 MeV	3.164 E+07	278.5	3.5096 E-05	1.546 E+04
2 MeV	4.136 E+08	47.18	3.5096 E-05	1.008 E+05
3 MeV	8.824 E+08	197.5	3.5096 E-05	4.221 E+05
4 MeV	4.875 E+08	457.85	3.5096 E-05	3.917 E+05
5 MeV	8.800 E+08	162.9	3.5096 E-05	2.516 E+05
6 MeV	1.220 E+09	115.59	3.5096 E-05	2.474 E+05

Table 7. Calculating the neutrons incident on the 1-L detector

5.3.2 Calculating Practical Efficiency

For 4-6 MeV, we may establish a practical efficiency, because the low energy peak does not interfere with the main higher energy peak. A rough estimate of the efficiencies for 4-6 MeV is listed below. These were determined from summing the counts in the peaks from Figure 13. We divided the counts in the peak by the total number of neutrons hitting the detectors, as determined by the TOF data. Error is within a few percent. Total efficiency uses all of the counts in all channels without cutoff.

Energy	Total Cnts	Pk Bins	Pk Cnts	Inc. n	Pk Eff.	% Er.	Total Eff.	% Er.
4 MeV	25561	2300-6100	20125	3.917 E+05	0.0514	0.70	0.0653	0.63
5 MeV	10952	2600-7000	8424	2.516 E+05	0.0335	1.09	0.0435	0.96
6 MeV	13855	2900-7200	10289	2.474 E+05	0.0416	0.99	0.0560	0.85

Table 8. Efficiency calculations for 4-6 MeV

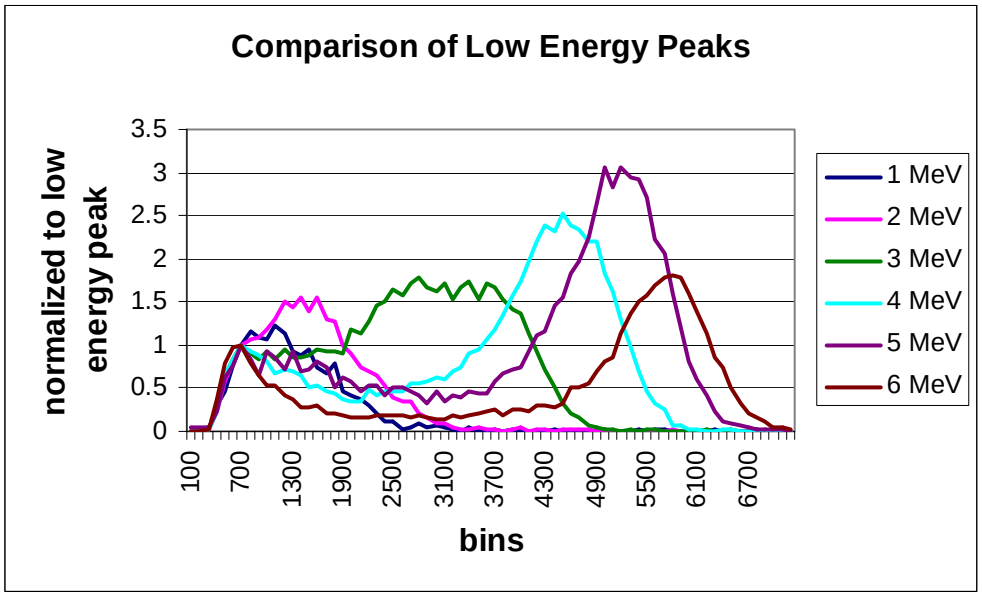

Figure 14. Data normalized to the low energy peak

These peak efficiencies in Table 8 reflect the counting efficiency of the detector above a certain threshold (see the third column of Table 8). This means that for future experiments with the 1-L detector, a threshold may be set to cut off the low energy pulses which would fall in the low energy peak. We would not be able to do this for 1-3 MeV

without a threshold device which allows the shape of the subtraction to be better defined. For example, with 4-6 MeV and a threshold at bin 2300, the efficiency at 4 MeV is as reported, and the efficiencies at 5 and 6 MeV would increase to 0.0345 and 0.0433, respectively.

5.3.3 Subtracting the Low Energy Peak

To subtract the low energy peak, I normalized the charts from Figure 14 to the peak channel of each peak, as determined from the 4-6 MeV data. We only use the 4-6 MeV data, as the lower energy runs have data overlapping the low energy peak. Notice the similarity in the peaks for three higher energies. To define the low energy peak we could choose a few different possibilities. The 6 MeV low energy peak has the least noise and lowest valley between the peaks, so it would be the most conservative approximation. We could also take an average of all three energies from 4-6 MeV, or take the most inclusive of the peaks. The problem with these approaches is that with this method of analysis the 1 MeV data peak is severely affected, dropping from larger than 600 neutrons in the first of these analyses to about 300 in the last. At that stage, noise takes over the shape of the peak, as the error changes by $1/\sqrt{N}$. Included are the first two low energy peak approximations.

Both of these approximations are smoothed artificially so that noise fluctuations are not magnified in the low energy peak subtraction. The conservative definition of the low energy peak does not remove the peak from the other energies, so it may be that that the middle definition is the most accurate. However, this means that the 1 MeV data has only 300 neutrons, which has 6 % statistical uncertainty. On the other hand, 600 neutrons correspond to 4 % statistical uncertainty. Another possibility to consider is that since 1

MeV data was taken with an amplifier, the low energy peak may not appear to be the same shape for 1 MeV as it does for the rest.

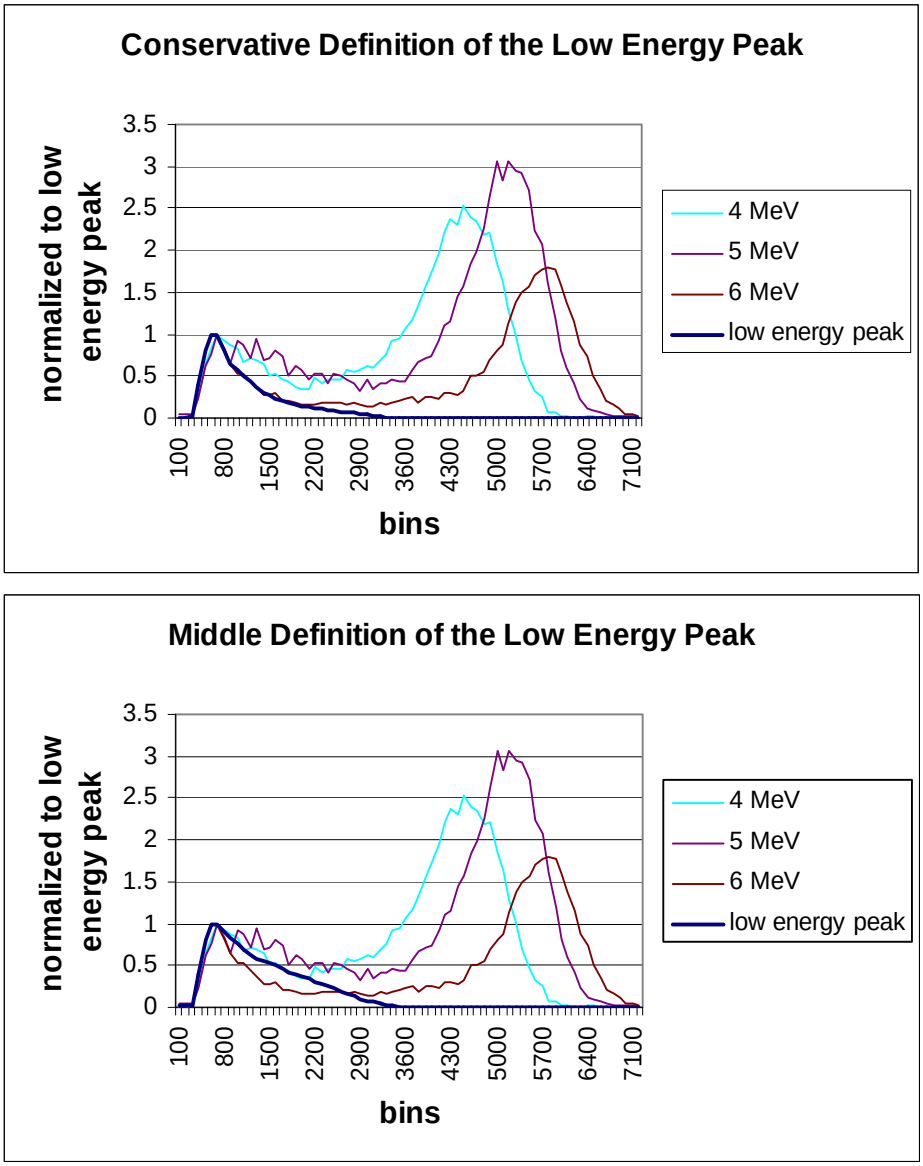

Figure 15. Low energy peak approximations

For this reason, I include both approximations for comparison. Both may be incorrect analyses, but we are merely attempting to determine the efficiency of the 1-L detector at each energy. Notice the residual low energy peak for the conservative

approximation for 3-6 MeV. Notice also the effect of the middle approximation on 1 MeV. Calculated efficiencies change accordingly, with most difference in 1 MeV and least for the high energies since we only take counts in the main peak, as described by range of channels.

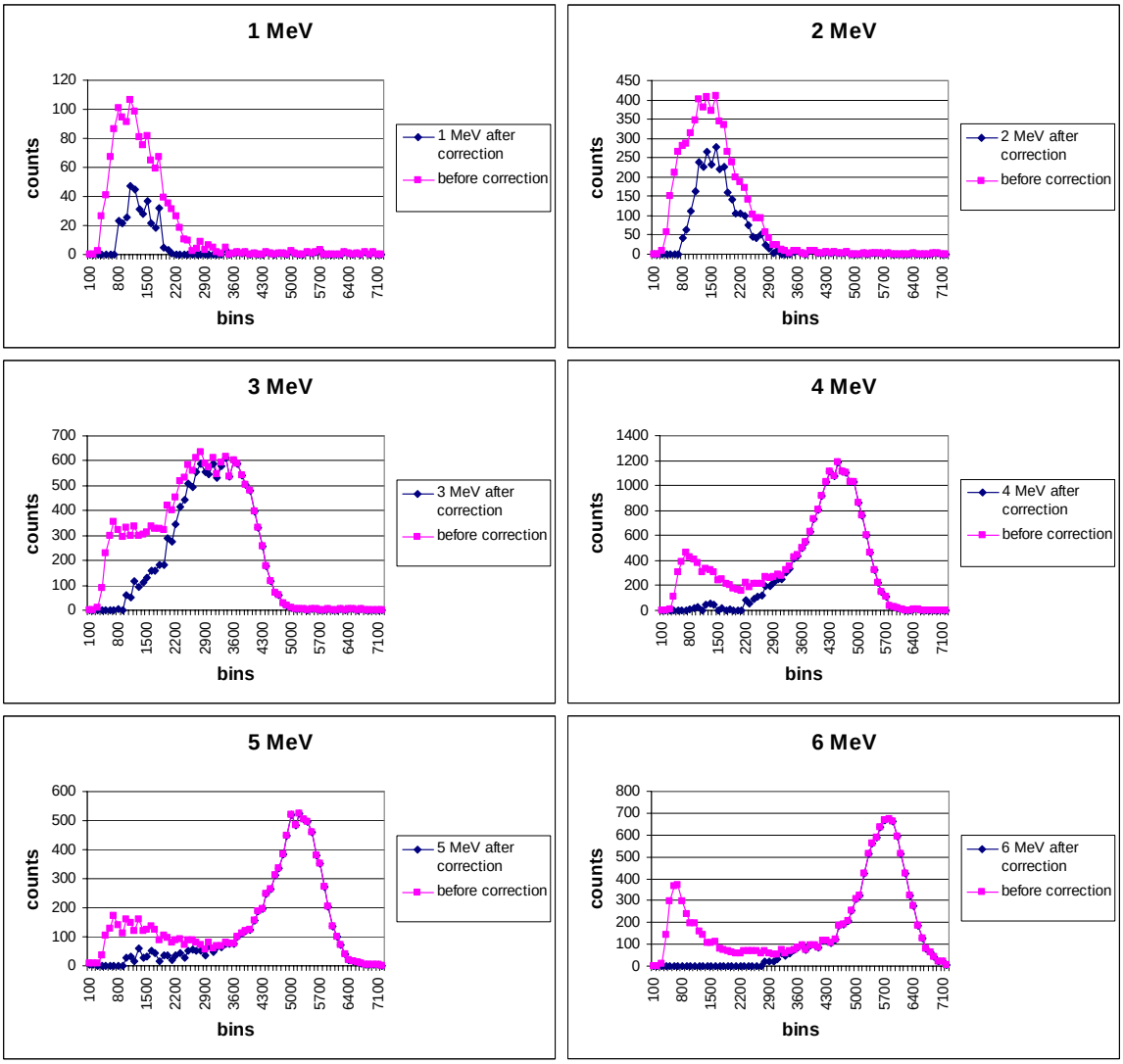

Figure 16. Middle approximation for low energy peak subtraction

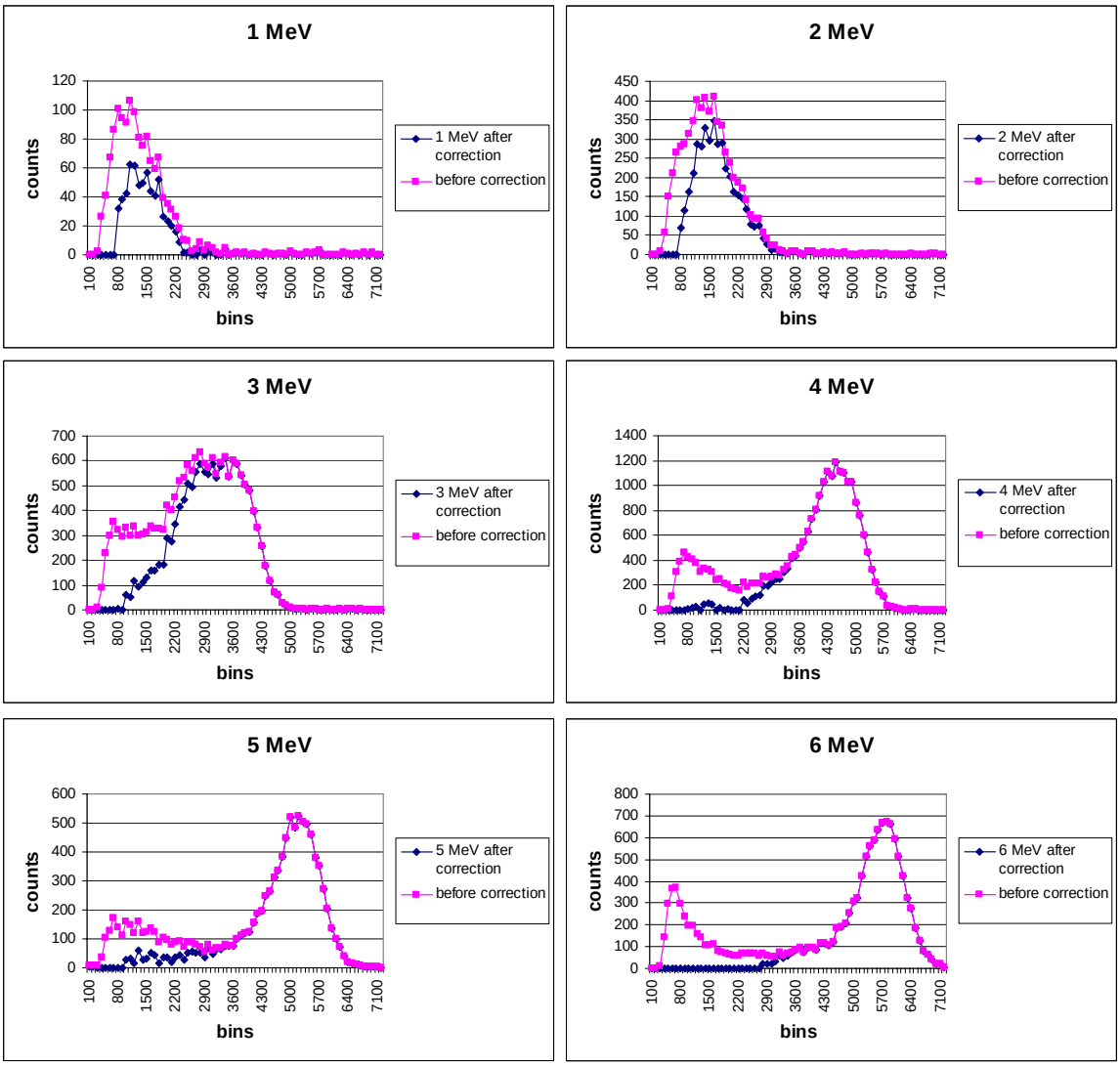

Figure 17. Conservative approximation for low energy peak subtraction

Below are two tables of these calculated efficiencies.

Energy	Counts in Peak	Peak Bins	Incident Neutrons	Efficiency	% Error
1 MeV	339.90	0-2600	1.55 E+04	0.022	5.42
2 MeV	2944.17	0-3300	1.01 E+05	0.029	1.84
3 MeV	13308.92	0-5300	4.22 E+05	0.032	0.87
4 NeV	19453.46	1700-5900	3.92 E+05	0.050	0.72
5 MeV	8328.81	2500-6800	2.52 E+05	0.033	1.10
6 MeV	10184.65	2700-7200	2.47 E+05	0.041	0.99

Table 9. Middle approximation calculated efficiencies

Energy	Counts in Peak	Peak Bins	Incident Neutrons	Efficiency	% Error
1 MeV	627.23	0-2600	1.55 E+04	0.041	3.99
2 MeV	4019.64	0-3300	1.01 E+05	0.040	1.58
3 MeV	14751.43	0-5300	4.22 E+05	0.035	0.82
4 MeV	20493.36	1700-5900	3.92 E+05	0.052	0.70
5 MeV	8428.38	2500-6800	2.52 E+05	0.033	1.09
6 MeV	10313.09	2700-7200	2.47 E+05	0.042	0.98

Table 10. Conservative approximation calculated efficiencies

Table 9 lists the efficiencies as calculated with the middle approximation for the subtraction of the low energy peak. Table 10 lists the efficiencies as calculated with the conservative low energy peak subtraction. Notice the difference of a factor of two for the 1 MeV calibrations. Looking at the MCNP calculations for lithium capture in the 1-L detector, we see that we expect a higher efficiency at low energies.

Since the MCNP calculated lithium capture efficiency as a function of energy drops off so quickly after 1 MeV, I choose the conservative approximation for the measured 1 MeV data analysis. This detector has been designed to enhance the efficiency around 4 MeV. We were not expecting that the efficiency would ever be higher around 4 MeV than at 1 MeV, because all MCNP plots for any lithium based detector show the same exponential decay as a function of energy. I think this is a good indication that the actual low energy peak is somewhere between the conservative and middle approximations, as 3 MeV for each one is similar, but one has 1 MeV efficiency

Figure 18. MCNP calculated lithium capture eff.

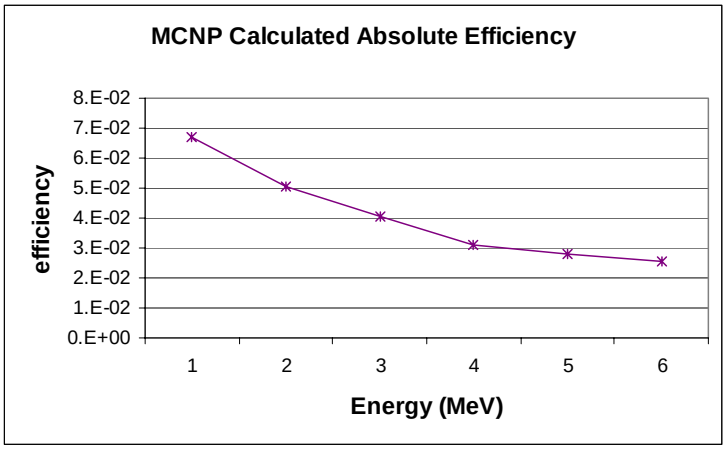

higher and the other lower than the 3 MeV efficiency.

There is a dip in efficiency at 5 MeV probably because of the influence of carbon inelastics. It is around 5 MeV that carbon inelastics begin to take energy away from the scintillator, and the hydrogen cross section is falling off [37].

5.3.4 Details of MCNP Modeling of Ohio Calibration

To model this system, we included the aluminum support for the 1-L detector, and the concrete to each side of the monitoring detectors. The source is modeled as a conical beam instead of point source or straight beam. This is a good approximation for the actual source in Ohio. For the spectrum recovery modeled by Sara Pozzi at ORNL, the spectrum from the TOF measurements were used. For more simple efficiency calculations we used the main energy peak value instead of the spectrum, and used enough incident neutrons to achieve good statistics. Errors listed are for the ratios.

Energy	MCNP Eff.	Subtr. Eff.	Subtr. Ratio	% Error	Total Eff.	Ratio	% Error
1 MeV	0.067	0.041	0.608	4.02	0.0893	1.337	2.69
2 MeV	0.050	0.040	0.791	1.65	0.0629	1.248	1.26
3 MeV	0.040	0.035	0.864	1.00	0.0422	1.044	0.75
4 MeV	0.031	0.050	1.594	0.96	0.0653	2.095	0.63
5 MeV	0.028	0.033	1.183	1.29	0.0435	1.556	0.96
6 MeV	0.025	0.041	1.625	1.22	0.0560	2.210	0.85

Table 11. Comparison of calculated efficiencies

We did not receive copies of Sara Pozzi's spectrum results, but she talked to us about the low energy peak as has been discussed previously. The efficiency calculations are in Table 11 which includes the ratio of the subtracted low energy peak efficiencies to the MCNP calculated efficiency, and the ratio of the efficiency calculated with the total counts in the data to the MCNP calculated efficiency. MCNP calculations include all lithium captures, with no threshold.

Note that the measured efficiencies with low energy peak subtraction are a compound of the conservative and middle approximations: 1-3 MeV are from conservative low energy peak subtraction, and 4-6 MeV are from middle low energy peak subtraction. Even with 1-3 MeV reported with a conservative subtraction, the ratio between measured and MCNP absolute efficiencies switches from below to above one. This supports my assumption that the conservative model is better for the low energies, especially 1 MeV. With the middle approximation, the ratio at 1 MeV would be 0.33. However, the total efficiency with no subtraction for 1-3 MeV is closer to MCNP than either subtraction approximation.

Even though the 4-6 MeV measured efficiencies are more trustworthy, they show much higher deviation from the MCNP ratio compared to the single glass detector using a californium calibration. The average of these three ratios with low energy peak subtraction is 1.47, significantly higher than the single glass ratio of 0.945. The total efficiency for 4-6 MeV is twice as large as MCNP.

Note also that MCNP fails to account for any drop in efficiency at 5 MeV as was measured in both the low energy peak subtraction and total efficiencies. Dr. Thomas Massey at OU assures me that a drop in efficiency at 5 MeV is normal, so unless there is something absorbing 5 MeV neutrons in their calibration room, I feel that our measured efficiencies are accurate.

5.4 Cross Talk Effects

To simulate two detectors next to each other, we took a plastic container with plastic scintillator in it and set it next to the 1-L detector during some measurements. The

data show no difference between these runs and those without the phantom detector, within the estimated uncertainties. This verifies that our detector does not exhibit substantial cross talk in this geometry. If cross talk contributed to the data, the number of counts detected would increase when the phantom was placed next to the detector. Any remaining cross talk is eliminated in this detector because we demand both a recoil and capture pulse from each detector. In the neutron-neutron scattering experiment all of the detectors involved would have this same feature, eliminating cross talk. The accidental coincidence data can include cross talk effects, but these effects can be subtracted out of the data in the same manner as has been done in the analysis for the calibration.

5.5 1 MeV Revisited

Because of the low efficiency at 1 MeV, we decided to supplement our calibration with data taken with a proton accelerator in the BYU underground laboratory. This accelerator is under the charge of Dr. Lawrence Rees. We used the tritium reaction $p+t \rightarrow n+{}^{3}He$ to produce 1 MeV neutrons from 1.8 MeV protons, as the Q value of the reaction is 0.76 MeV. This system is not well characterized in room return, nor does it have the capability of providing the necessary information for an absolute efficiency calculation. The benefit of this study is merely to look at the shape of the response function.

In February 2005 we set up the detector 48.3 cm from the tritium target and 106.7 cm off the floor. We took data totaling above 7000 counts, but as the incident number of neutrons is unknown, we were only able to use data acquisition rates to analyze the spectra. We had a background run with the beam off but no run with the beam on but the detector out of the beam. This would have enabled us to approximate the room return.

The data was taken with the digitizer into Comread. This file was sent through Evecon to allow the appropriate lithium capture time window. Data and accidentals were analyzed in the same time frames as the previous Ohio calibration, for both background and 1 MeV data. Accidentals were subtracted from both of these runs. To plot the spectra we had to convert the data into rates by dividing by the livetime for each run, and then subtracting the background as a rate from the data acquisition rate. This yields spectra similar in many ways to the 1 MeV spectra from Ohio.

Figure 19. 1 MeV revisited with the BYU proton accelerator

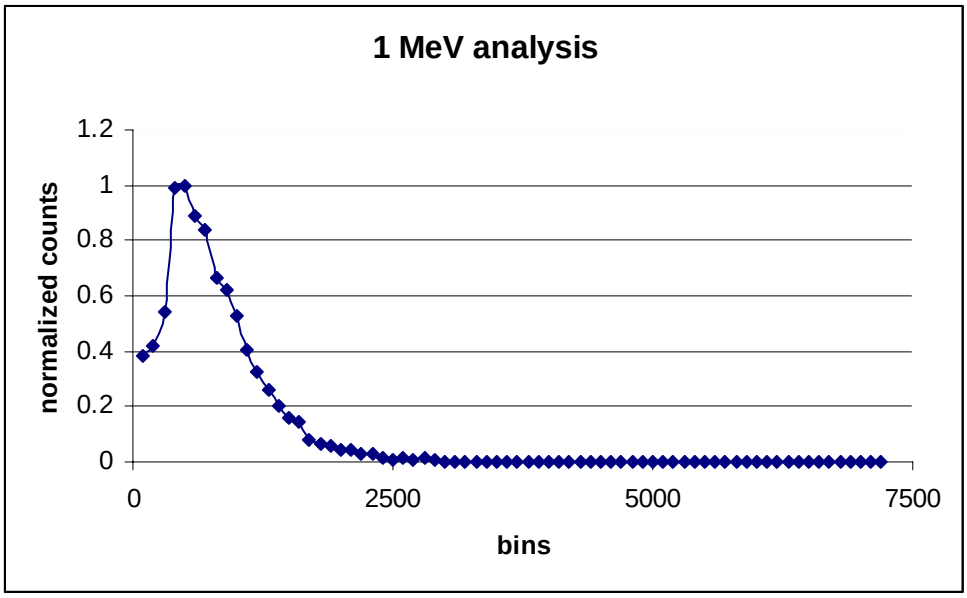

Here we see the same steep left side and more gently sloping right side of the peak. Like the 1 MeV data from Ohio with the low energy peak included, the maximum occurs before channel 1000. Since the low energy peak is believed to be intrinsic to the detector, this is expected in any 1 MeV data analyses.

6. Preliminary n-n Scattering Experiment

6.1 Setup

In March of 2005 we returned to Ohio to set up system with two detectors for the neutron-neutron scattering length measurement. We took the two 1-L detectors as described in Section 2, a LeCroy digitizer and the appropriate power supplies for all equipment. We also borrowed a deuterated benzene active target from Charles Hurlbut of Ludlum Measurements Inc in Sweetwater Texas. This is because the active beryllium target never showed data above background with 10 MeV neutrons. (Tom Massey sent us the background and data files before the second trip so that we could plan an alternate target.)

For this experiment, the n-n scattering system was run behind the n-p scattering system being used by Ohio University. They are using 14 MeV neutrons from the $d+d \rightarrow n+{}^{3}He$ reaction, of which many pass straight through their system, and are an appropriate energy for the $n+d \rightarrow n+n+p$ reaction used for the n-n scattering length measurement. This will yield a kinematic peak at 5.5 MeV in the detected n-n neutrons, according to Kesmecketi et al [38,39]. This is within the range of our previous calibrations, although a calibration at 10 MeV would be a helpful supplement.

The system was set up in a large room adjacent to the accelerator room, with beamlines entering in through the wall. We set up the deuterated benzene target in an adjustable mounting device 2 meters back from the n-p experiment. The detectors were set up on a fixed frame 166.4 cm from the floor, the height for the deuteron beam. These detectors were at a 30 degree angle relative to the deuteron beam direction so that we could avoid incident neutrons from the $d+d \rightarrow n+{}^{3}He$ reaction, and only study neutrons

coming from the reaction n+d→n+n+p as the target emits neutrons isotropically. Neutrons from the n-p experiment were removed by two towers of paraffin directly in between the 1-L detectors and the n-p scattering site. The 1-L detectors were placed in contact with each other, 2.667 m away from the benzene target so that small differences in angle for the two neutrons coming out of the reaction could be detected. This is because the n-n scattering length effect is more apparent for two neutrons traveling in nearly the same direction.

The PMTs used were all ETL tubes, with 1300 V on the first detector, 1100 V on the second so that the lithium capture peak would occur in the same channel on SCOPE. The active benzene target also had 1300 V on the PMT, high enough for the electronics to be sensitive to each pulse.

An electronics triggering system was designed to trigger on the coincidence of a benzene signal followed by a pulse from either of the two detectors, using the dynodes of the PMT. This trigger was used with the LeCroy digitizer with the two channels connected to the anodes of the two detectors. All cables used were brought into the control room with low resistance wires.

6.2 Component Details

6.2.1 Lanthanum Beryllate Target

The proposed active target consists of a beryllium compound, lanthanum beryllate, with chemical formula $La_2Be_2O_5$. Lanthanum beryllate releases alphas from the immediately decaying ^{8}Be and neutrons from the reaction $n+^{9}Be \rightarrow n+n+^{8}Be$. The target is 3 cm in diameter, 1 cm thick. The cross section for the 10.0 MeV incident

neutrons on beryllium-9 is 0.53 barns. The active target pulses enable us to easily compute the energies of the detected neutrons, using the alphas as a time zero and the detected neutrons as the stop time. Beryllium-8 has a half life of 7×10^{-17} seconds, so the alpha particles are essentially released instantaneously from the reaction $n+{}^{9}Be \rightarrow n+n+{}^{8}Be$. A PMT is glued directly onto the target, so that the light emitted from the lanthanum beryllate scintillator is detected immediately, and provides a start pulse for the time of flight calculations.

The Q-value for the $n+{}^{9}Be \rightarrow n+n+{}^{8}Be$ reaction is 92 keV, which would produce alpha particles at half this energy. These are low energies and would not provide scintillation pulses visible above background. Theoretically, random low-energy background neutrons do not provide enough energy to create a start pulse. The scintillator pulses from reactions triggered by the incident 10 MeV neutrons will have a pulse area corresponding to the approximately 5 MeV alpha particles.

The problem, as mentioned previously, is that the target, though active, did not produce any measurable difference in background from 10 MeV neutrons. We will investigate this problem at a later time. We spoke with Dr. Charlotte Ester at Ohio University, a theoretical nuclear physicist. She assures us that the problems encountered in a theoretical analysis for the $n+{}^{9}Be \rightarrow n+n+{}^{8}Be$ reaction would be large enough that the nucleon scattering community would not trust a measurement obtained with that reaction anyway. She also assures us that the discrepancy in the neutron scattering length has been studied with every possible theoretical angle, with no satisfactory results. She assumes that the problem then lies in the experiment, which is quite probable.

6.2.2 Deuterated Benzene Target

The benzene target, C_6D_6, is 98 % by weight deuterated benzene, and 2 % organic fluors. It is housed in a cylindrical plastic container. The inner height and inner diameter are 2 inches. The benzene was put directly onto a 2 inch PMT. The plastic container has a total height and outer diameter of 2 ¼". These were placed inside a black plastic container designed to shield a PMT from external light. The fluor produces light scintillation whenever the n+d→n+n+p reaction occurs.

6.2.3 Electronic Triggering System

To design the triggering system we took pulses from the dynodes of the benzene PMT and also from each detector. Each is fed into an Ortec 454, which is a timing filter amplifier. The benzene pulses were sent into an Ortec 473, and the detectors signals were sent into Ortec 583s, which are all constant fraction discriminators. From there, each was directed into Ortec 416A gate and delay generators, set to minimum delay. A logic circuit is then constructed with the aid of Phillips Scientific Model 754B, which is a quad four-fold logic unit. We take the benzene pulse and either one of the detectors. The output of this unit is sent to an inverter before going to the LeCroy digitizer.

To describe what is happening to the shape and size of the pulses at each stage: the dynode produces positive pulses, and the constant fraction discriminators require negative pulses so the timing filter amplifiers are used to invert the signal as well as amplify it to be high enough for the discriminators to recognize them. The output of the discriminators is very narrow, only 20 ns wide, and it is a discriminator because it can filter out noise by the pulse height requirement. One option for output on the discriminators is to use an adjustable width. The gate and delay generator allowed us to

use a wide gate for the benzene and narrow for the detectors to suppress noise. The logic circuit produces a negative output but the LeCroy digitizer demands a positive signal so an inverter is used to correct this.

The advantage of using a logic gate in the triggering system is it eliminates 99 % of the events which would occur each time the benzene triggered, without requiring a coincidence with a pulse in either detector. It helps the data analysis then, in preselecting events which include at least two of the required pulses, by only triggering when the benzene and either detector yield a pulse. Ideally the events will have a trigger pulse to mark time zero for the time of flight, and then two sets of recoil and capture pulses, one for each of the two neutrons from the reaction n+d→n+n+p. These neutron capture events may occur in separate detectors or in the same detector.

6.2.4 LeCroy Digitizer

The LeCroy digitizer is powered by a portable Camac crate, which has a readout into a PCMCIA card. This card is read by the laptop with a program named Acquire. It has three inputs: trigger and two channels. The trigger is defined through the electronics system in the previous section. The two channels are occupied by the pulses from the anodes of the two 1-L detectors. When the trigger fires the PCMCIA card reads the pulses in either of the two channels, as directed by the program Acquire.

6.2.5 Acquire

This program and the Camac crate are similar to Comread and the Buehler boards. It is specialized to communicate with a PCMCIA card in the laptop computer. An input file, test.con, describes the allowed time between pulses, the time to add before the interval gate, and pulses characteristics for SCOPE. The event files are analyzed with

SCOPE. For a dual neutron experiment, a new version of SCOPE is needed to keep track of the two neutrons. We will also need to relate the LeCroy data acquisition to the Buehler board digitizer acquisition performed for the calibrations.

6.3 Preliminary Data

In setting up this system, we used a 5 Ci plutonium-beryllium source over the benzene target. The beamline for the n-p experiment was under repair and we were unable to run with monoenergetic neutrons. However, with a hot radioactive source, enough neutrons hit the detectors to make a few coincidences with benzene, and each detector. We call a gold event one in which an n+d→n+n+p reaction occurs in benzene, followed by both detectors giving a start and stop pulse. A silver event is one in which we have three of these pulses. The pulses we need for analysis are the two recoil pulses for the two neutrons, but having those capture pulses is important to make sure that the recoil pulses represent all of the incident energy. In a few runs with the plutonium source we found a few silver events.

7 Future Developments

7.1 d-d Measurement at 2.5 MeV

The purpose of making a d-d reaction measurement is to check the nuclear accelerator at Ohio. Since we no longer trusted MCNP as a check, we wished to check the Ohio calibration experimentally. We should get the same efficiency for the same energy, no matter the source. By using the associated particle method for calibration, we eliminate the need to know the lithium cross-section in the detector. We only need to know the counts in the lithium capture peak and divide it by the total flux. The 2.45 MeV incident neutrons produce a lithium capture peak at approximately 7.0 MeV. Zero energy neutrons would produce that peak at 4.8 MeV. The lithium peaks are shifted in energy because of the energy of its decay products, an alpha and a triton. We can calculate the precise neutron energy in the lab frame from kinematics of the d-d reaction. The Q-value (available energy in the lithium alone) is also well known. Thus if we use a d-d measurement and then compare the results with a 2.5 MeV calibration, we will have a check on the accelerator, one which could be used at any facility to test its accuracy.

7.2 A 10 MeV Calibration

As mentioned previously, a 10 MeV calibration would ease the analysis of the dual neutron scattering experiment, as our current maximum is 6 MeV and the peak for n+d→n+n+p is at 5.5 MeV [38,39]. While 10 MeV is being used, it would also be helpful to study the pulses from the lanthanum beryllate target to see if we can recognize any problems with the system used previously, or if the target itself is deficient.

7.3 Preliminary Scattering Data Analysis

To date the n-p scattering experiment at Ohio University has not been run except for background. Since our experiment is run in conjunction with their n-p scattering experiment, we will take data in tandem. We expect more data in June, at which point we will know more about the efficiency of a dual neutron study with these detectors, as well as the assurance that this system is appropriate for use in a dual neutron scattering experiment. We will need to create another version of SCOPE for the data analysis.

Appendix 1: MCNP Code Example and Explanation

The basic elements of the code are, in order: defining the cells; defining the surfaces; defining the materials, temperature, and energy; tally cards describing the reaction to be counted and in what manner it is to be counted. The file has comment cards describing lines, marked by $ for comments, and c to skip that line. This file is from a model of a californium point source incident on the 1-L detector.

```
c
  1   51  -1.03     -10  -2  1          $first column is cell number, then material number,
  2   53  -2.5      -25  -3  2          $density in g/cm3, and then the volume as described
  3   51  -1.03     -10  -4  3          $by positive or negative respect to surfaces
  4   53  -2.5      -25  -5  4
  5   51  -1.03     -10  -6  5
  6   53  -2.5      -25  -7  6
  7   51  -1.03     -10  -8  7
  8   50  -2.5      -10  -26  9
  9   57  -1.18      1  -26  10  -11
 10   55  -2.7       12  -26  13  -14
 11   57  -1.18     -11  -1  12
 12   56  -8.9       16  -15  -21  22  19  -20
 13   56  -8.9       17  -18  -21  22  19  -20
 14    0  12  -26  -13  11
 15   55  -2.7       -14  -12  24        $the # symbol means not that cell number
 17    0  -23   #1 #2 #3 #4 #5 #6 #7 #8 #9 #10 #11 #12 #13 #14 #15 #19
 18    0  23
 19   58  -0.87      1  -9  -10   #1 #2 #3 #4 #5 #6 #7

  1      py      0.7          $surfaces: py indicates a plane in the y direction
  2      py      3.7          $note all distances are in centimeters
  3      py      3.8
  4      py      7.6
  5      py      7.7
  6      py     11.5
  7      py     11.6
  8      py     15.4
  9      py     16.3
 10      cy     6.64         $cy is a cylinder about the origin, the number following
 11      cy        7         $describes the radius
 12      py        0
 13      cy      9.3
 14      cy     9.62
```

```
  15      px     -9.9
  16      px      -10
  17      px     19.9
  18      px       20
  19      pz      -12
  20      pz    13.12
  21      py       74
  22      py      -74
  23      so      100          $so stands for sphere about origin
  24      py    -0.16
  25      cy     6.35
  26      py  16.6175

mode  n                        $neutron mode, following are material cards
m51   6012.            9       $Plastic
     1001.           10
m53   14000.          0.189 $Li-glass
     8016.          0.605 3006.          0.189 3007.          0.008
     12000.         0.002 13027.         0.007
m55   13027.           1 $Aluminum
m56   26000.           1 $Iron (steel)
m50   8016.         -0.465 $PMT glass
     14000.        -0.327 13027.        -0.005 12000.        -0.042
     20000.        -0.05 11023.         -0.111
m57   6012.            5 $plexiglass
     8016.          2 1001.            8
m58   6012.           20 $Mineral oil
     1001.           22
imp:n  1         15r       0         1   $ importances (how MCNP tracks neutrons)
tmp1   2.55e-008      17r               $ temperature
sdef  POS=0 -62.46 0 CEL=17 ERG=D1 TME=0 WGT=1  PAR=1 $Californium source
si1   H 0.015 0.035 0.055 0.075 0.095 0.115 0.135 0.165 0.195      $pos=position,
     0.225 0.255 0.305 0.355 0.405 0.455 0.505 0.555 0.605         $erg=energy, cel=cell
     0.655 0.705 0.755 0.805 0.855 0.905 0.955 1.05 1.15
     1.25 1.35 1.45 1.55 1.65 1.75 1.85 1.95 2.15
     2.35 2.55 2.75 2.95 3.25 3.55 3.85 4.15 4.45
     4.75 5.05 5.55 6.05 6.55 7.05 7.55 8.05 8.55
     9.05 9.55 10.05 10.55 11.05 11.55 12.05 12.55
     13.05 13.55 14.05 14.6 15.9 16.9 17.9 19.1 20.0
sp1   D 0 1.98e-3 2.64e-3 3.13e-3 3.54e-3
     3.88e-3 4.18e-3 6.75e-3 7.25e-3 7.67e-3
     8.04e-3 1.41e-2 1.48e-2 1.54e-2 1.58e-2
     1.61e-2 1.64e-2 1.66e-2 1.67e-2 1.68e-2
     1.68e-2 1.68e-2 1.68e-2 1.67e-2 1.66e-2
     3.12e-2 3.23e-2 3.15e-2 3.07e-2 2.98e-2
     2.88e-2 2.77e-2 2.67e-2 2.56e-2 2.46e-2
```

```
     4.60e-2 4.20e-2 3.81e-2 3.44e-2 3.10e-2
     4.07e-2 3.44e-2 2.89e-2 2.42e-2 2.02e-2
     1.68e-2 1.39e-2 1.80e-2 1.31e-2 9.48e-3
     6.83e-3 4.90e-3 3.52e-3 2.52e-3 1.81e-3
     1.29e-3 9.26e-4 6.62e-4 4.73e-4 3.38e-4
     2.41e-4 1.72e-4 1.23e-4 8.75e-5 6.21e-5
     4.78e-5 6.15e-5 2.12e-5 1.06e-5 6.01e-6
     2.15e-6
f4:n  (2 4 6)                  $tally on cells 2,4,6 (lithium glass)
fm4:n -1 53 105                $tally the reaction number 53 (lithium capture)
t4    50 100 200 400 800 1600 3200 6400 12800          $time bins for tally (shakes)
     25600 51200
e4    1.0e-4 1.0e-3 1.0e-2 1.0e-1 1.0 2.0 3.0 4.0 5.0       $energy bins for tally (MeV)
     6.0 7.0 8.0 9.0 10.0 15.0
phys:n  15
nps   100000000                          $number of particles
print -20 -32 -35 -80 -85 -86 -90 -98 -110 -120 -128 -130 -160 -161 -162
```

Appendix 2: SCOPE Manual

This is the operation manual I wrote for SCOPE. This program was written with the intent to make it available to other scientists researching neutron detection.

SCOPE Program Operation Manual

File

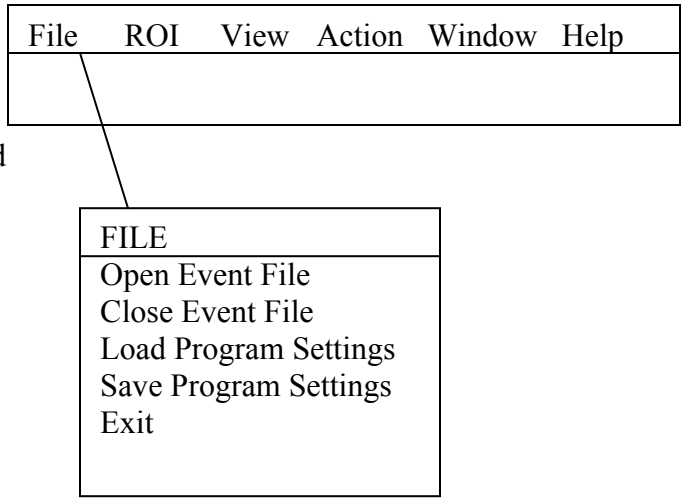

Open Event File

Click on Shortcut to New Acquired Data. Select the appropriate file to analyze data.

Close Event File

Closes the opened file.

Load Program Settings

Change the program settings.

Save Program Settings

Save existing settings.

Exit

Close SCOPE.

ROI

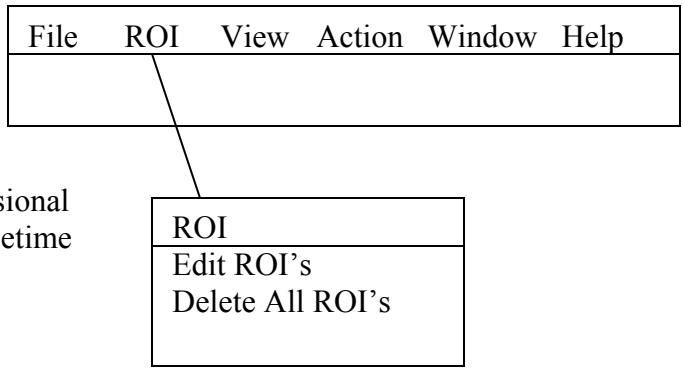

Select a Region of Interest (ROI) by click-dragging a box in the area of a two-dimensional data plot of Early/Late, Width, or Max Risetime (see VIEW for details).

Edit ROI's

To define the region use the left, right, top, and bottom parameters, which will alter the ROI selected on a plot, if any exist. Choose the plot between Early/Area by Area, Pulse Width, and Max Delta Y. Choose the color of the region of interest by clicking on the "Choose Color" button. Select a color option and pressing "OK." The "Delete" button will delete the selected ROI in the Scatter box. "Make New" will add another ROI. Select an ROI to set parameters for that ROI. Click on "OK" when finished, then R and G to see the ROI(s) in the selected color(s) on the scatter plot.

Delete All ROI's

Erases all previously defined region of interest parameters.

View

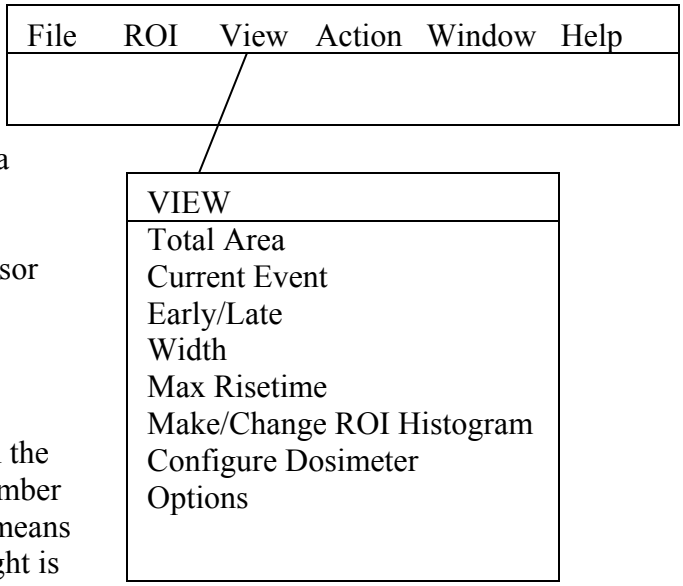

Total Area

This screen displays a graph of area projected on the x-axis. Left click for the left cursor, right click for the right cursor. Area listed is the area between the two cursor positions.

Current Event

Above the digitized event is shown the event number, time index, pulse count (number of pulses in a specified timeframe). POS means starting time position. (Ignore Valid) Height is the pulse height; width is the full width at half-maximum; length is display length of a single pulse in microseconds; and norm area is the area above a defined baseline.

When double events occur, the difference in time position is (second pulse time – 20.37 :s) for the length of time between pulses.

Early/Late

A graph with early area by total area on the y-axis by the area on the x-axis. To display type R (Restart Analysis) and G (Go).

Width

A graph with the pulse width at full width half-maximum on the y-axis by the area on the x-axis. Press R then G to display.

Max Risetime

A graph of the steepest part of the slope of the pulse on the y-axis and the area on the x-axis. Press R then G to display.

Make/Change ROI Histogram

Scatter Plots allows the choice of plots to use for the histrogram. The graph must be already in existence. For Histogram View, horizontal projects the points against the x-axis, vertical projects them against the y-axis. ROI's in Scatter Plot liss number of neutrons and spikes, which are high-energy gammas. The Y Scale allows options for data analysis. "None" is plotted without altering the scale. ROI must be defined for a histogram.

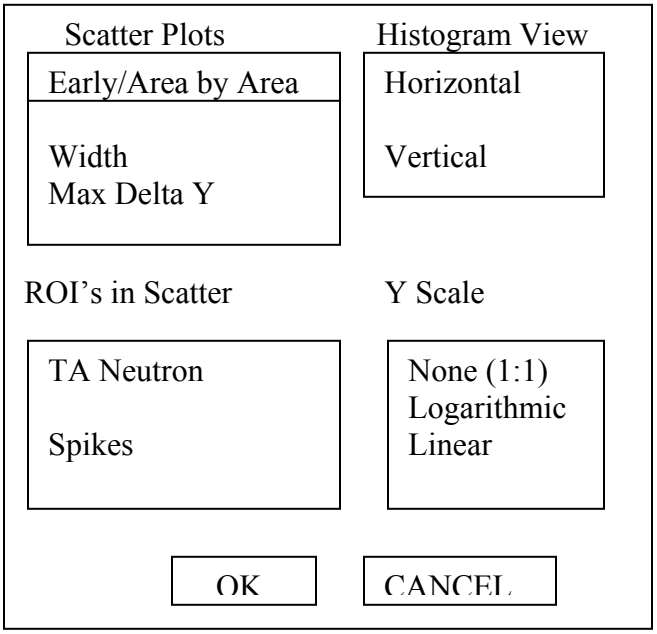

Configure Dosimeter

To display, press R, then G. The ROI must have been defined previously. Proton Recoil Spectrum P+A (MeV Neutrons) are the number of events that are doubles (proton collisions + neutron capture in lithium of Region A).

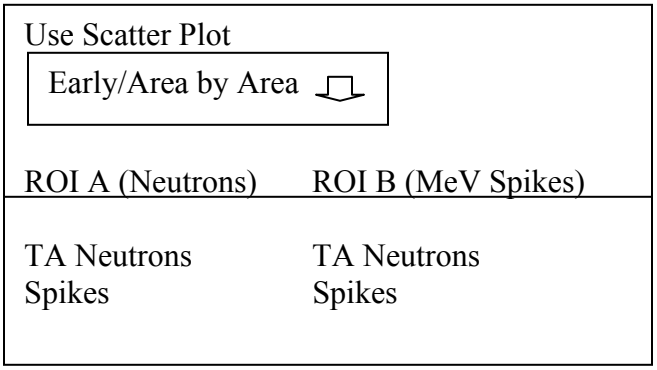

Options

Configure Options window has Total Area, Current Event, and Save in Settings as tabs.

Total Area

Defines x-scale and y-scale. The x-scale has minimum cutoff, maximum sutoff, and number of bins. Maximum cutoff is the number of total area bins displayed

in the histogram. The default setting is (0, 5000, 500) respectively. The y-scale has options none and linear for data presentation. The buttons "Restore Defaults" and "Restore Previous" are for manipulations of the x-scale settings.

Current Event
Displays options and preview. Options allow settings for base line, early/late cut, and saturation cutoff. There is also a checkbox for "reject events with multiple pulses in the same microsecond." The baseline determines how much background is subtracted from a single event. Early/late cut determines the time division between the early and late portions of each event. Saturation cutoff also has a checkbox for activation and signifies pulse rejection by maximum amplitude level. The default settings are (13.750, 20, 246) respectively.

Save in Settings
This window lists saved parameter options with checkboxes.

- Regions of Interest
- Window Layout
- Total Area Histogram
- Current Event Configuration
- Save Current Settings on Exit

The default has all items checked except the last one.

Action

The Action window lists commands for the program, some of which have been mentioned in the VIEW section. In addition to those listed, S means Stop.

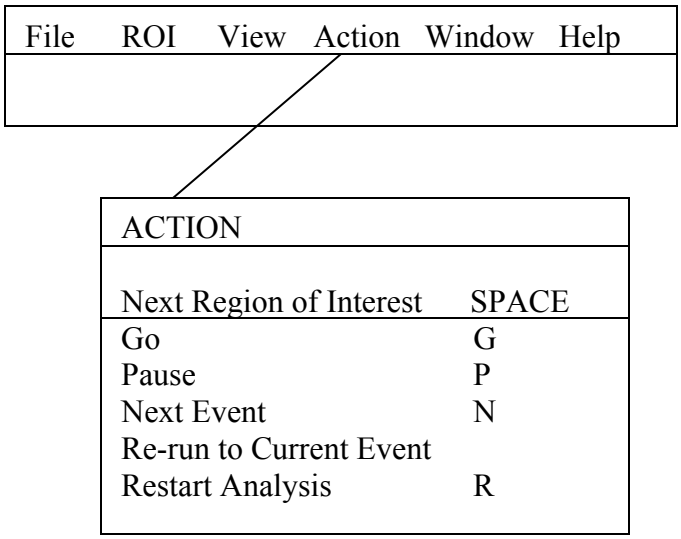

Window

Window lists typical options. The list (numbered) at the bottom are the windows that are currently open. Current Event and Early/Area are open upon starting SCOPE.

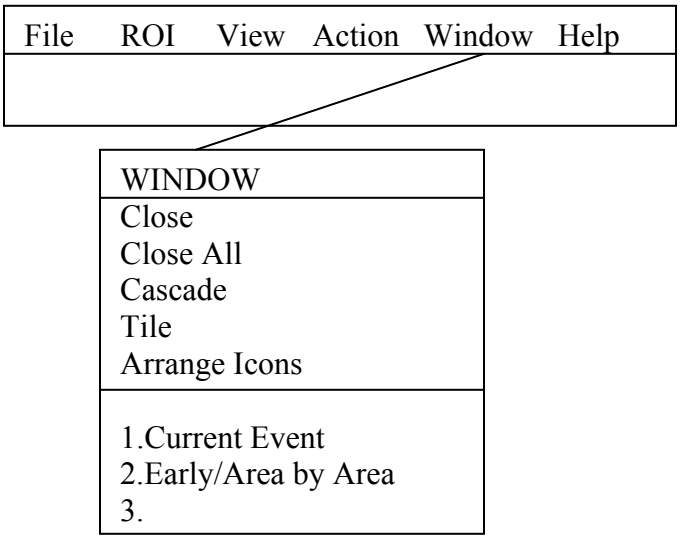

Help

"About" just leads to copyright information with program writer Tom Abbott to whom questions may be directed.

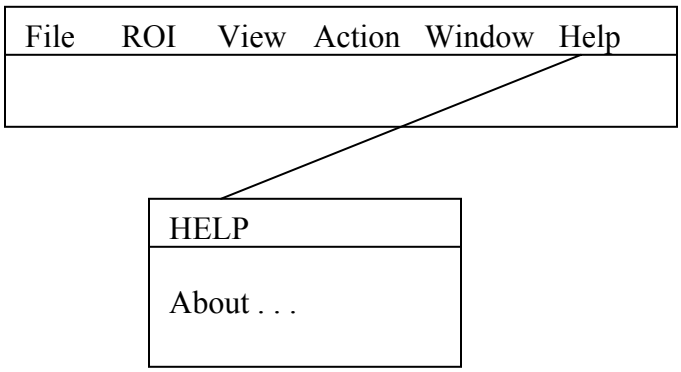

References

1. P. E. Hodgson, E. Gadioli, and E. Gadioli Erba, *Introductory Nuclear Physics*, Oxford Science Publications (1997).
2. I. Šlaus, Y. Akaishi, and H. Tanaka, Neutron-Neutron Effective Range Parameters, Phys. Reports 173 (1989) 257.
3. W. I. Furman, et al., J. Phys. G: Nucl. Part. Phys. 28 (2002) 2677.
4. L. Heller, P. Signell, and N. R. Yoder, Phys. Rev. Lett. 13 (1964) 577.
5. D. R. Nygren, A Measurement of the neutron-neutron scattering length, Ph.D. Thesis (1968).
6. M. Bander, Phys. Rev. 134 (1964) B1052.
7. C. R. Howell, et al., Phys. Lett. B 444 (1998) 252.
8. G. A. Miller, B. M. K. Nefkens, E. Šlaus, *Charge Symmetry, Quarks, and Mesons*, Phys Reports 194 (1990) 1.
9. K. Watson, Phys. Rev. 88 (1952) 1163.
10. E.I. Sharapov, et al., Direct Measurement of Neutron-Neutron Scattering, Proceedings of the 17th International Conference on the Application of Accelerators in Research and Industry, Denton, Texas, edited by Jerome L. Duggan and I. L. Morgan, Melville, NY AIP (2003).
11. R. Grötzschel, et al., Nucl. Phys. A176 (1971) 261-272 and references.
12. K. Bodek, et al., Few-Body Systems 8 (1990) 23 and references.
13. V. Huhn, et al., Phys. Rev. C 63 (2000) 014003.
14. D. E. G. Trotter, et al., Phys. Rev. Lett. 83 (1999) 3788.
15. M. W. McNaughton, et al., Nucl. Phys. A239 (1975) 29.

16. I. Šlaus, Y. Akaishi, H. Tanaka, Phys. Rev. Lett. 48 (1982) 993.

17. M. Allet, et al., Few-Body Systems 20 (1996) 27.

18. A. Nogga, et al., Phys. Rev. C 67 (2003) 034004.

19. W. Tornow, et al., Phys. Rev. C 54 (1996) 42.

20. K. W. McVoy, Phys. Rev. 121 (1961) 1401.

21. W. von Witsch, *Can the Neutron-Neutron Scattering Length be Determined from n-d Breakup Experiments?*, Proceedings of the 17th International Conference on the Application of Accelerators in Research and Industry, Denton , Texas, edited by Jerome L Duggan and I. L. Morgan, Morgan, Melville, NY (2003) AIP.

22. O. Schori, et al., Phys. Rev. C 35, (1987) 2252.

23. B. Gabiould, et al., Nucl. Phys. A420 (1984) 496.

24. R. M. Salter, et al., Nucl. Phys. A254 (1975) 241.

25. B. Zeitnitz, et al., Nucl. Phys. A231 (1974) 13.

26. B. Gabiould, et al., Phys. Rev. Lett. 42 (1979) 1508.

27. K. Bodek, et al., Few-Body Systems 3 (1988) 135.

28. H. Witala, et al., Phys. Rev. C 51 (1995) 1095.

29. W. Tornow, R. T. Braun, H. Witala, Phys. Lett. B 318 (1993) 281.

30. H. Jeremie, R. Larose-Poutissou, Phys. Lett. 44B (1973) 68.

31. J. B. Czirr, G. L. Jensen, Nucl. Inst. Met. Phys. Res. A 349 (1994) 532.

32. J. B. Czirr, priv. comm.

33. Los Alamos National Laboratory, Documentation for CCC-200/MCNP Code Package, MCNP: Monte Carlo Neutron and Photon Transport Code System 3.A, Los Alamos, NM, (1983).

34. J. B. Czirr, et al., Nucl Inst Meth A 476 (2002) 309.

35. S. Pozzi, priv. comm.

36. S. A. Pozzi, E. Padovani, M. Marseguerra, MCNP-PoliMi: A Monte-Carlo code for correlation measurements, Nucl. Instrum. Methods A 513/3, (2003) 550.

37. D. I. Garber, R. R. Kinsey, Nuclear Cross Section 3rd edition vol. 2, (1976).

38. J. Kecskeméti, T. Czibók, B. Zeitnitz, Nucl. Phys. A254 (1975) 110.

39. J. Kecskeméti, T. Czibók, Phys. Rev. Lett. 32, (1974) 1063.